

IVO ROMET

Recombination luminescence
of doped borates: origin and application
prospects in dosimetry



IVO ROMET

Recombination luminescence
of doped borates: origin and application
prospects in dosimetry



UNIVERSITY OF TARTU
Press

This study was carried out at the Institute of Physics, University of Tartu, Estonia.

The dissertation was admitted on May 10, 2017, in partial fulfilment of the requirements for the degree of Doctor of Philosophy in materials science, and was allowed for defence by the Scientific Council on Material Science of the Institute of Physics, University of Tartu.

Supervisors: Dr. Vitali Nagirnõi
Institute Physics, University of Tartu, Estonia

Opponent: Dr. Anatoli Popov
Institute of Solid State Physics, Riga, Latvia

Defence: June 27, 2017, at University of Tartu, Estonia



European Union
European Regional
Development Fund



Investing
in your future

ISSN 2228-0928

ISBN 978-9949-77-455-5 (print)

ISBN 978-9949-77-456-2 (pdf)

Copyright: Ivo Romet, 2017

University of Tartu Press

www.tyk.ee

CONTENTS

LIST OF PUBLICATIONS INCLUDED IN THE THESIS	7
LIST OF ABBREVIATIONS	9
1. INTRODUCTION	10
2. GENERAL BACKGROUND	12
2.1. Lithium tetraborate applications	12
2.2. Crystal structure of $\text{Li}_2\text{B}_4\text{O}_7$	13
2.3. Photoluminescence and TSL results on $\text{Li}_2\text{B}_4\text{O}_7$	14
3. EXPERIMENTAL	18
3.1. Preparation of the investigated samples	18
3.1.1. Single crystals	18
3.1.2. Ceramics	18
3.2. Methods and equipment	19
3.2.1. Photoluminescence	19
3.2.2. Radioluminescence and cathodoluminescence	21
3.2.3. Thermostimulated luminescence	21
3.2.4. Electron paramagnetic resonance study	22
4. RESULTS AND DISCUSSION	23
4.1. Spectral characteristics of impurity ions and their position in lattice	23
4.1.1. $\text{Li}_2\text{B}_4\text{O}_7\text{:Cu}$	23
4.1.2. $\text{Li}_2\text{B}_4\text{O}_7\text{:Ag}$	24
4.1.3. $\text{Li}_2\text{B}_4\text{O}_7\text{:Cu,Ag}$	26
4.1.4. $\text{Li}_2\text{B}_4\text{O}_7\text{:Mn}$ crystals and ceramics	27
4.1.5. Mn^{2+} ions localization in the $\text{Li}_2\text{B}_4\text{O}_7$ lattice	30
4.1.6. Comparison between crystal and ceramic $\text{Li}_2\text{B}_4\text{O}_7\text{:Mn}$	36
4.1.7. Influence of the X-ray irradiation	36
4.2. Low temperature radioluminescence and cathodoluminescence of crystalline samples	37
4.3. Low-temperature TSL curves and lattice dynamics	38
4.4. TSL spectra and dosimetric properties	44
4.4.1. $\text{Li}_2\text{B}_4\text{O}_7\text{:Cu}$	44
4.4.2. $\text{Li}_2\text{B}_4\text{O}_7\text{:Ag}$	45
4.4.3. $\text{Li}_2\text{B}_4\text{O}_7\text{:Cu,Ag}$	46
4.4.4. $\text{Li}_2\text{B}_4\text{O}_7\text{:Mn}$ single crystal	47
4.4.5. $\text{Li}_2\text{B}_4\text{O}_7\text{:Be}$, $\text{Li}_2\text{B}_4\text{O}_7\text{:Mn}$ and $\text{Li}_2\text{B}_4\text{O}_7\text{:Mn,Cu}$ ceramics	51
4.4.6. Controlling dosimetric performance of ceramics by preparation methods	56
SUMMARY	58
SUMMARY IN ESTONIAN	60

ACKNOWLEDGEMENTS	62
REFERENCES	63
PUBLICATIONS	69
CURRICULUM VITAE	105
ELULOOKIRJELDUS	108

LIST OF PUBLICATIONS INCLUDED IN THE THESIS

The current thesis is based on the following publications, which are listed below by the Roman numerals from **I.** to **IV.**

- I.** M. Kerikmäe, M. Danilkin, A. Lust, V. Nagirnyi, L. Pung, A. Ratas, **I. Romet**, V. Seeman, “Hole traps and thermoluminescence in $\text{Li}_2\text{B}_4\text{O}_7\text{:Be}$ ”, *Radiation Measurements*, **56** (2013) 147–149.
- II.** V. Nagirnyi, E. Aleksanyan, G. Corradi, M. Danilkin, E. Feldbach, M. Kerikmäe, A. Kotlov, A. Lust, K. Polgár, A. Ratas, **I. Romet**, V. Seeman, “Recombination luminescence in $\text{Li}_2\text{B}_4\text{O}_7$ doped with manganese and copper”, *Radiation Measurements*, **56** (2013) 192–195.
- III.** **I. Romet**, E. Aleksanyan, M.G. Brik, G. Corradi, A. Kotlov, V. Nagirnyi, K. Polgár, “Recombination luminescence of Cu and/or Ag doped lithium tetraborate single crystals”, *Journal of Luminescence*, **177** (2016) 9–16.
- IV.** **I. Romet**, M. Buryi, G. Corradi, E. Feldbach, V. Laguta, É. Tichy-Rács, V. Nagirnyi, “Recombination luminescence and EPR of Mn doped $\text{Li}_2\text{B}_4\text{O}_7$ single crystals”, *Optical materials*, accepted manuscript.

AUTHOR'S CONTRIBUTION

Author's contribution to each research paper is given in the list below:

- I.** The author was responsible for thermostimulated luminescence measurements and analysis, for post-processing of the previously recorded data and preparation of figures for publication.
- II.** The author was responsible for thermostimulated luminescence measurements and analysis, for post-processing of the previously recorded data and preparation of figures for publication.
- III.** The first author of publication, was responsible for thermostimulated luminescence measurements and data analysis as well as for literature data investigation, participated in writing the manuscript and preparation of the figures presented in the article, largely contributed to literature data investigation in order to explain the results on experimental data.
- IV.** The first author of publication, was responsible for providing most of the measurement data and post processing of the acquired data as well as for analysis of the results and preparation of the figures. Initiated the EPR studies, wrote the first version of the manuscript, largely contributed to literature data investigation in order to explain the results on experimental data.

OTHER PUBLICATIONS OF THE DISSERTANT

These following publications are not related to the subject matter of the thesis:

- V. A. Kuznetsov, A. Frorip, J. Kozlova, V Nagirnyi, M. Ots-Rosenberg, **I. Romet**, A. Sünter, “Visible fluorescence of biological fluids as a renal failure marker: New integrative approach”, *Journal of Innovative Optical Health Sciences*, **8** (4) (2015) 1550030.
- VI. I. E. Seferis, K. Fiaczky, D. Spassky, E. Feldbach, **I. Romet**, M. Kirm, E. Zych, “Synthesis and luminescence properties of BaHfO₃:Pr ceramics”, *Journal of Luminescence*. In Press:
<http://dx.doi.org/10.1016/j.jlumin.2016.09.035>
- VII. V. Kortov, A. Lushchik, V. Nagirnyi, D. Ananchenko, **I. Romet**, “Spectrally resolved thermally stimulated luminescence of irradiated anion-defective alumina single crystals”, *Journal of Luminescence*. **186** (2017) 189-193.

LIST OF ABBREVIATIONS

CCD	charge-coupled device
CL	cathodoluminescence
e	electron
EPR	electron paramagnetic resonance
h	hole
HFS	hyperfine structure
LTB	$\text{Li}_2\text{B}_4\text{O}_7$, lithium tetraborate
NIR	near-infrared
PL	photoluminescence
PMT	photomultiplier tube
RL	radioluminescence
RT	room temperature
SHG	second harmonic generation
SR	synchrotron radiation
STE	self-trapped exciton
TLD	thermoluminescence dosimeter
TSL	thermostimulated luminescence
UV	ultraviolet
Vis	visible range
VUV	vacuum ultraviolet

1. INTRODUCTION

Thermally stimulated luminescence (TSL) is the property of irradiated material to emit light at heating below the incandescent temperature. The ionizing irradiation dislodges electrons in insulators or semiconductors, creating hot electrons in the conduction band and holes in the valence band, some of which will become self-trapped or trapped at lattice imperfections. Sample heating provides enough energy for charge carriers to become mobile and recombine giving rise to luminescence.

There are numerous properties which are sensitive to irradiation induced changes in the crystal electron energy and lattice structure such as light absorption, fluorescence, phosphorescence, dielectric constant, magnetic susceptibility, catalytic activity etc. Purposeful modifications of impurity concentration, synthesis and crystallization techniques and following physical treatments can substantially enhance the sensitivity of selected crystal characteristics to radiation. Up to now, TSL has been recognized as the most sensitive and reliable tool for measuring the irradiation dose of materials exposed to various kinds of ionizing radiation. Since the first proposal to use TSL for radiation dosimetry [1], a huge research effort has been put in the development of dosimetric materials with improved performance. Various types of dosimeters have been developed and proposed for thermoluminescence application. Lithium and calcium fluorides doped with one or more impurities are the most common dosimeters provided by different manufacturers. The former, when enriched with ^6Li isotope, is used for gamma and neutron detection, while the latter is more frequently used for measuring the dose of gamma radiation. Also other compounds like beryllium oxide, calcium sulphate, lithium tetraborate ($\text{Li}_2\text{B}_4\text{O}_7$) doped with various impurity ions are used for specific dosimetric applications. The majority of commercially available dosimeters are produced in a form of powders or sintered pellets. Although, powders have a lower light yield compared to crystals due to light scattering within the material, their features are easily reproducible due to the averaging of the heterogeneity in the specimen. Easy reproducibility and low cost are the main reasons why these types of thermoluminescence dosimetry (TLD) materials are used up to date.

In the past few decades, lithium tetraborate based dosimeters in different forms (powders, ceramics, single crystals), doped with one or more impurities, have attracted tremendous attention in science and medicine for human-tissue equivalent radiation dose monitoring. When doped with manganese or copper, this material exhibits some desirable features like high sensitivity exceeding that of well-known TLD-100 (LiF:Mg,Ti) [2]. Recently $\text{Li}_2\text{B}_4\text{O}_7\text{:Mn}$ was demonstrated to be an efficient dosimetric material with excellent γ dose linearity and negligible fading on storage [3]. It is important to note that the majority of the most recent TSL studies have been carried out on complex ceramic compounds co-doped with other impurities such as phosphorus, copper, indium etc. [4], which made the interpretation of the possible mechanisms responsible for

recombination processes rather controversial. The present thesis is an attempt, based on a large variety of spectroscopic measurements, density function calculations, and EPR studies to obtain a more reliable interpretation of the elementary processes of photoemission and recombination luminescence taking place in undoped lithium tetraborate ($\text{Li}_2\text{B}_4\text{O}_7$, or LTB) as well as lithium tetraborate doped with single impurities of Cu, Ag, Mn, and Be or their combination.

The main aims of the work are:

- To investigate in detail photostimulated and thermostimulated luminescence and to reveal the nature of luminescence centres and mechanisms responsible for energy storage and thermostimulated luminescence in doped lithium tetraborate.
- To find proper conditions such as doping and co-doping ion type and optimum concentration, synthesis route and sample post-treatment for enabling the development of a doped lithium tetraborate with improved sensitivity to ionizing radiation.

In order to achieve goals set, the specific subtasks were fulfilled:

1. Synthesis of doped and co-doped lithium tetraborate ceramics and their characterisation.
2. Photostimulated luminescence study of undoped and doped single crystals and ceramics in wide temperature range 2–800 K at excitation energies 3–20 eV in order to characterize the luminescence centres in the materials studied.
3. EPR study of doped crystals and ceramics and the characterisation of impurity ion incorporation in the $\text{Li}_2\text{B}_4\text{O}_7$ lattice.
4. Thermostimulated luminescence study of undoped and doped crystals and ceramics in wide range of temperatures 5–700 K in order to clarify the recombination mechanisms responsible for the dosimetric properties of the material.
5. Determination of thermal stability of charge carrier trapping centres relevant for recombination luminescence.

2. GENERAL BACKGROUND

2.1. Lithium tetraborate applications

During the recent 30 years, a considerable amount of research and development has been focused on borate based materials mainly because of their high potential in a large variety of technical applications briefly listed below. For a long time one of these materials, lithium tetraborate, has attracted a particular attention due to high stability of its optical properties as well as wide transparency range extending down to 160 nm in vacuum ultraviolet (VUV) region, thus exceeding other known nonlinear optical materials such as LiNbO_3 , LiIO_3 , and KTiOPO_4 [5–7]. It has been shown by Ogorodnikov [8] that this material has a wide band gap of ~ 9 eV, which makes it suitable for doping with various transition and rare earth metal ions. It has been recognized as an important material suitable for generation of second to fifth harmonics from a high powered Nd:Y₃Al₅O₁₂ laser [6, 9, 10], and as a frequency conversion material for high powered UV solid state lasers, based on second harmonic generation and sum frequency generation of the visible laser radiation [11, 12]. The damage threshold of $\text{Li}_2\text{B}_4\text{O}_7$ crystal is ~ 40 GW/cm² (fused silica 10 GW/cm² [6]), which exceeds the threshold for other types of borates several times over [7]. Since it possesses a high electromechanical coupling factor k^2 and a low temperature coefficient of frequency it has been considered as a suitable substrate material for surface acoustic wave devices in TVs and other devices using modern day signal processing techniques [13–15]. LTB has been recognised as a promising material suitable also for piezoelectric and pyroelectric sensor development [16–17]. It also has been known as an ionic conductor due to the high mobility of Li^+ ions along the [001] type axis at high temperatures [18–21]. Some parameters relevant for the above-described applications are shown in Table 1.

From the time of Daniel's proposal to use thermostimulated luminescence for a radiation dosimetry [1], a tremendous effort has been put into development of new phosphors with improved performance for this application. The first introduced phosphor material suitable for radiation dosimetry was $\text{Li}_2\text{B}_4\text{O}_7\text{:Mn}$ [22]. However, several drawbacks have been mentioned such as the emission band peaking at 600 nm (which was out of the range of contemporary photomultipliers), poor TSL intensity, limited dose linearity and noticeable fading. These shortcomings were partially overcome by replacing manganese with copper [23], resulting in an emission at about 360 nm. It has been shown later that LTB samples synthesized by different methods (powders, ceramics, transparent glasses and single crystals) and doped with various metal ions demonstrate an outstanding sensitivity exceeding that of the well-known LiF:Mg,Ti (TLD-100) [2, 24, 25]. If ^6Li and ^{10}B isotopes are incorporated into the LTB crystal, it becomes a potential TLD material suitable for fast and thermal neutron detection by means of scintillation method [2, 26–28]. The effective atomic number (Z_{eff}) of lithium tetraborate is 7.3, which closely

matches with the Z_{eff} of soft human tissue (7.42) and therefore, it has been recognised as a tissue equivalent TSL material [22, 29, 30]. In addition, the energy response of LTB in the range 15–100 keV is similar to that of soft tissue, making it attractive also for radiology diagnostics [31]. Only few tissue equivalent materials are suitable for dosimetry, particularly in clinical applications and radiation therapy.

Table 1. Physical properties of $\text{Li}_2\text{B}_4\text{O}_7$.

Density (g/cm^3)	2.45 [32]
Point group	C_{4v} (4mm) [33]
Piezoelectric stress constant, $[\text{C}/\text{m}^2]$	$e_{15}=0.324$; $e_{31}=0.148$; $e_{33}=0.800$ [15]
Cell dimensions [\AA]	$a=9.477$ $c=10.286$ [33]
Refractive indices	$n_o=1.592$ $n_e=1.538$ [33]
SHG coefficients $[\text{pm}/\text{V}]$	$d_{31}=0.073$ $d_{33}=0.55$ [34]
Transparency $[\text{nm}]$	170–3500 [6]
Damage threshold $[\text{GW}/\text{cm}^2]$	~ 40 (10 ns) [6]
SHG cutoff $[\text{nm}]$	487 [6]
Remarks (phase matching properties for type I SHG); $\Delta\theta$ $[\text{mrad}\cdot\text{cm}]$, ΔT $[\text{°C}\cdot\text{cm}]$	1064 \rightarrow 532 $\theta=32.0^\circ$ $\Delta\theta=0.048$ $\Delta T=21.0$ [35]

2.2. Crystal structure of $\text{Li}_2\text{B}_4\text{O}_7$

$\text{Li}_2\text{B}_4\text{O}_7$ synthesized in non-single crystalline form is a white powder-like material with a calculated density found to be close to $2.4 \text{ g}/\text{cm}^3$ [32, 33]. Naturally occurring lithium tetraborate is known as the mineral diomignite, which is transparent, colorless and extremely rare in nature [36]. The melting point of LTB has been determined at 917 °C [37]. The crystal structure of lithium tetraborate has been for the first time calculated and reported by Krogh-Moe in 1962 [33]. At room temperature (RT), the crystal structure is characterized by the non-centrosymmetric, tetragonal space group $I4_1cd$ (C_{4v}^{12}), possessing 104 atoms per unit cell with a dimensions $a=b= 9.479(\pm 0.003) \text{ \AA}$, and $c= 10.280(\pm 0.004) \text{ \AA}$, and having a polar axis parallel to the $[001]$ crystallographic direction [38]. According to [39], LTB forms a so-called carcass structure due to a rigid anion sublattice composed of a 3-dimensional boron-oxygen network. In the LTB structure, there are boron ions in both trigonal and tetrahedral positions in the surrounding environment of three or four O^{2-} ions, respectively (Fig. 1). The main structural element of the lithium tetraborate is a boron-oxygen complex $[\text{B}_4\text{O}_9]^{6-}$, consisting of two planar

trigonal BO_3 and two tetragonal BO_4 molecules (Fig. 1b). The average B-O interatomic distance was found to be around $\sim 1.48 \text{ \AA}$ for tetragonal complex and 1.367 \AA for the trigonal complex [39, 40]. These trigonal and tetragonal complexes are combined by common bridging oxygen atoms into spirals with a symmetry axis of [001] direction. The spirals themselves are connected via one of the common bridging oxygens, belonging to a trigonal BO_3 complex. The Li^+ ions stabilizing oxyanionic frame are located in the cavities of the B-O spirals and within the distorted tetrahedra composed of four close oxygen atoms (Fig. 1a). The interatomic distance between the four closest oxygens and lithium has been found to be ranging from 1.97 to 2.14 \AA , while between two lithium ions it is 3.114 \AA [38, 39]. The ionic radii and valences for different ions in the $\text{Li}_2\text{B}_4\text{O}_7$ crystal are as follows: Li^+ (0.68 \AA), B^{3+} (0.20 \AA), and O^{2-} (1.32 \AA).

Recently the bond lengths and angles between the atoms were determined even more accurately as function of temperature in the range of $3.4\text{--}1200 \text{ K}$ [41–43].

All these crystal structure data are important for the analysis of impurity incorporation into the lattice and revealing the processes responsible for recombination luminescence in doped LTB.

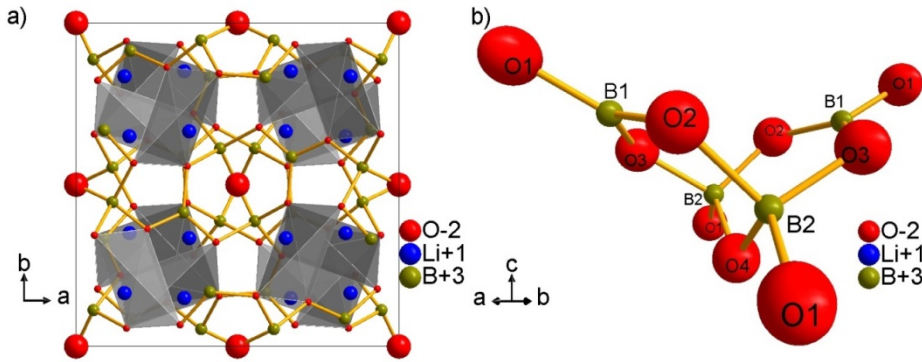


Fig. 1. a) The structure of $\text{Li}_2\text{B}_4\text{O}_7$ depicted within one unit cell as a parallel projection along the [001] direction, showing also the Li-O polyhedron (filled with a gray color) forming a fourfold screw axes in the lattice. The right panel **b)** is a representation of the main cradle-like (B_4O_9) motif in LTB crystals. It is projected along the [110] - type axis in order to visualize the two BO_3 and two BO_4 structural network units (boron atoms are marked respectively, as B1 and B2). These structure images are based on the results obtained by [39].

2.3. Photoluminescence and TSL results on $\text{Li}_2\text{B}_4\text{O}_7$

The photoexcitation of undoped LTB crystals in the narrow energy region $8\text{--}10 \text{ eV}$ above the fundamental absorption edge has been shown to lead to electronic transitions from oxygen to boron oxyanionic states, forming self-

trapped excitons (STEs), which decay radiatively, resulting in a broad characteristic STE emission at 3.65 eV (see, e. g., [8, 44] and references therein). The STE formation efficiency is much lower under excitation at higher energies above 10 eV. Thermostimulated luminescence studies carried out on undoped LTB crystals at high temperatures have revealed a TSL glow peak with maximum at 194 °C (467 K, heating rate 5 K/s), demonstrating a relatively weak gamma sensitivity [2]. However, thermally and optically stimulated luminescence have been known to be most sensitively dependent on the interplay between the host intrinsic properties and its defect structure, a particular role being played by impurities providing charge trapping levels in the bandgap. For that reason, doped LTB has become a most extensively studied material in view of potential dosimetric applications.

A number of various impurities such as Cu, Ag, P, Eu and Mn have been used to create in LTB trapping and luminescence centres relevant for dosimetry [2, 3, 4, 22, 24, 25, 30]. Depending on doping and preparation methods some materials revealed an extraordinary radiation sensitivity [24] or dose response linearity [3]. The properties of the Cu impurity in $\text{Li}_2\text{B}_4\text{O}_7$ have been described for two of its charge states populating the crystal [45]. By the EPR studies it has been found that Cu^{2+} ions substitute on a strongly distorted Li site, while the Cu^+ ion derived from the dynamics of its low temperature photoemission properties, has been demonstrated to occupy at low temperatures an off-centre position of C_2 symmetry close to Li^+ site. Two groups of excitation bands centered at 5 and 7 eV have been revealed in the excitation spectrum of the Cu^+ emission and ascribed to the $3d^{10} \rightarrow 3d^9 4s$ and $3d^{10} \rightarrow 3d^9 4p$ transitions, respectively [45]. Despite the strong overlap between the STE and Cu^+ emission bands they can be easily distinguished due to the substantially smaller half-width of the Cu^+ emission band. The high-temperature TSL studies have shown that two glow peaks situated at 380 and 500 K are observed in LTB:Cu, their positions being strongly affected by sample preparation, heating rate, and irradiation methods [25, 46–48]. The situation becomes even more complex when co-dopants are used [24, 48–50].

Far less studies have been published on the spectroscopic properties of LTB:Ag. This material has been reported to display an emission band at slightly different positions peaking at 272 nm (4.56 eV), 280 nm (4.43 eV), or 264 nm (4.7 eV) [51–53]. Only the long-wavelength edge of the excitation spectrum has been reported for this emission, revealing a band peaking at 206 nm (6.02 eV). The observed emission and excitation bands have been tentatively ascribed to the $4d^9 5s \leftrightarrow 4d^{10}$ transitions of the Ag^+ ions, although no experimental or theoretical verification of the origin of this emission has been performed [52, 53]. A TSL band of LTB:Ag corresponding to this emission has been described around 150–165 °C, its position also depending on the heating rate [47, 48, 54]. The majority of the TSL experiments has been carried out on complex ceramic compounds co-doped also with other impurities such as phosphorus, copper, indium etc. [4, 48, 55], which made the interpretation of

the possible mechanisms responsible for recombination processes rather controversial.

Among other impurities manganese has been of special interest in view of the possibility of adapting the material dosimetric properties by varying doping methods and impurity concentration. Already the first introduction of LTB as a material suitable for radiation dosimetry has been based on the study of $\text{Li}_2\text{B}_4\text{O}_7\text{:Mn}$ phosphors by Schulman et al [22]. It seems to be generally accepted that manganese enters the LTB crystal lattice in the divalent state. The emission of Mn^{2+} ions peaking at about 608 nm in LTB crystals and a series of excitation bands in the region of 200–500 nm have been attributed to the transitions within the $3d^5$ electron configuration of the ion [52]. The same emission and the main excitation bands are well recognized also in glassy LTB doped with manganese [52, 56].

Thermally stimulated luminescence of LTB:Mn has been studied in single crystals, glasses and polycrystalline samples [47, 56–59, 60–62]. Most measurements have been conducted in the high-temperature range in order to identify the recombination processes responsible for the dosimetric peak. Only Podgórska et al. [56, 57] investigated TSL glow curves in the low temperature range from 10 to 310 K. At least five TSL peaks at about 95, 110, 130, 165 and 215 K have been distinguished in this region and assigned to certain types of traps present in the crystal bulk. In general, TSL peak positions and shapes in LTB doped with divalent manganese depend largely on synthesis process, irradiation dose and heating rate, and for that reason, their interpretations remain controversial, this being especially true for the high-temperature range [3, 60, 62]. Two complex peaks in the regions of 373–403 and 498–538 K (the second one peaking at about 510 K for a heating rate of 0.5 K/s) have been reported in ref. [60]. The position of the main peak has been reported at 498 K for a heating rate of 1 K/s in ref. [47]. In ref. [59] its position has been found at 477 K for the same heating rate. Finally, in polycrystalline samples, the position of the dosimetric peak has been given as 583 K and 551 K for heating rates 4 K/s [61] and 5 K/s [62], respectively.

Two main mechanisms have been proposed for the processes responsible for the dosimetric TSL peak in LTB:Mn. One approach considers, as a result of irradiation, the recharging of manganese ions mainly substituted for lithium, leading to the creation of Mn^{3+} ions which recombine with thermally released electrons, giving rise to Mn^{2+} emission in the dosimetric TSL process [47, 52, 56, 57, 62]. In another model, Mn^{2+} ions substituting for both lithium and boron, serve as traps for electrons and holes, respectively, while the emission is mainly due to recombination of thermally released holes near a manganese ion with subsequent energy transfer to the latter [63, 64]. Recharge processes are considered in this model only at the stage of high irradiation doses, when the dose dependence becomes nonlinear. The choice between these two models depends largely on the decision about the substitution site of Mn^{2+} in the LTB lattice, which in turn may depend on material morphology (powder, ceramics,

crystal), preparation method and, due to aggregation tendencies, also on impurity concentration.

There has been no consensus, concerning the position of Mn^{2+} in the LTB lattice. Earlier X-band EPR studies on glassy and single crystal LTB:Mn samples led to the suggestion that Mn^{2+} ions occupy Li^+ sites in deformed octahedral oxygen environments [56, 65]. Other EPR data were tentatively attributed to Mn^{2+} ions possibly substituting at boron sites of tetrahedral coordination [63, 64, 66]. Distinguishing between the various options is difficult due to the complex character of X-band EPR spectra excluding quantitative analysis.

There are some, mostly indirect and/or ambiguous data, indicating the presence of manganese ions in other valence states in LTB. These mainly concern EPR and optical absorption studies of irradiated samples. A sequence of absorption bands in the region of 200–620 nm have been related to various ions ranging from Mn^+ to Mn^{6+} [56–58, 67, 68]. The decrease of luminescence [52] and EPR [63] signals of Mn^{2+} centres have been detected in heavily irradiated single crystal and ceramic samples, indirectly indicating recharge processes with the formation of manganese ions in valence states other than divalent.

3. EXPERIMENTAL

3.1. Preparation of the investigated samples

Single LTB crystals and ceramics synthesized in three different ways were investigated in the context of the current thesis.

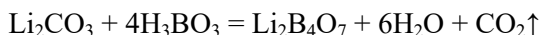
3.1.1. Single crystals

A set of undoped (pure $\text{Li}_2\text{B}_4\text{O}_7$) and differently doped ($\text{Li}_2\text{B}_4\text{O}_7\text{:Cu}$, $\text{Li}_2\text{B}_4\text{O}_7\text{:Ag}$, $\text{Li}_2\text{B}_4\text{O}_7\text{:Cu,Ag}$ and $\text{Li}_2\text{B}_4\text{O}_7\text{:Mn}$) single crystals were grown by the diameter controlled Czochralski method at the Institute for Solid State Physics and Optics, Wiegner Research Centre for Physics, Budapest, Hungary, using the 99.999% purity $\text{Li}_2\text{B}_4\text{O}_7$ powder. The concentration of the Ag and/or Cu and Mn dopants added as oxides of the corresponding purity to the melt was 0.5 mol%. However, only a small amount of dopant was incorporated into the crystals. According to atomic absorption analyses, the final concentrations of copper and silver were approximately 5×10^{-3} mol% each in $\text{Li}_2\text{B}_4\text{O}_7\text{:Cu}$, $\text{Li}_2\text{B}_4\text{O}_7\text{:Ag}$, and $\text{Li}_2\text{B}_4\text{O}_7\text{:Cu,Ag}$ crystals. The Mn doped crystal contained only 1.1×10^{-4} mol% of Mn^{2+} ions.

3.1.2. Ceramics

All sintered ceramic samples were prepared at the Institute of Chemistry, University of Tartu according to the two different procedures described below.

- In the first case lithium tetraborate was obtained by the reaction:



Binding agent SiO_2 (about 2 wt. %) was added to deionized water together with boric acid and heated at stirring. Lithium carbonate was added to a hot solution (80°C) of boric acid in small portions at continuous stirring.

To produce $\text{Li}_2\text{B}_4\text{O}_7$ doped with Cu, Mn or Be, the powders of CuSO_4 , MnCO_3 or BeO , respectively, were added to $\text{Li}_2\text{B}_4\text{O}_7$ typically in amounts of 0.13–0.26 mol% at the stage of the initial synthesis in water suspension under continuous stirring and heating of the mixture. The corresponding amounts are taken as impurity concentrations in the samples. The residual water and CO_2 were removed by annealing the mixture at 823 K for 120 min under constant nitrogen flow. The resulting material was ground in a mortar, and tablets were pressed. The ceramic tablets were sintered at various temperatures below the melting point of lithium tetraborate at 1190 K. The diameter of the sintered tablets was 4.5 mm.

- In the second procedure, lithium tetraborate was obtained similarly to the previous method, however, the doping was performed by using KMnO_4 in two different ways: either by adding a water solution of KMnO_4 (0.25 mol% relative to $\text{Li}_2\text{B}_4\text{O}_7$) to the hot solution of boric acid before the reaction with lithium carbonate or by adding it steadily drop-wise during the reaction.

When all components were added, continuous heating and stirring was performed at 75–85°C until the reaction between boric acid H_3BO_3 and Li_2CO_3 was completed, and the mixture became paste-like and difficult to stir. The obtained precursor was aged for 30–50 minutes at 80°C, then transferred to a smooth plate, and dried at 105°C during 12 hours. After that it was annealed at 575°C for 2 hours under flowing protecting inert gas to remove any H_2O and CO_2 traces. The precursor was then crunched, ground, and sifted to obtain the powder suitable for forming detectors. The detector tablets were molded with a percussive press from the precursor, and then placed on a smooth inert surface in the quartz tube located inside the furnace. The ceramic detectors were sintered under flowing protecting inert gas at the temperature in the range of 910–915°C during 45 minutes. The obtained ceramics were very hard semi-transparent ceramic bodies, molded in the form of tablets 0.8 mm thick and 4.5 mm in diameter. Doping with manganese by adding a water solution of KMnO_4 in one portion yielded relatively strong manganese clustering due to efficient co-precipitation of manganese probably forming the core of inceptive microcrystals of $\text{Li}_2\text{B}_4\text{O}_7$, while the drop-wise adding resulted in the material with manganese uniformly distributed in the lattice.

3.2. Methods and equipment

3.2.1. Photoluminescence

The steady-state photostimulated luminescence studies were carried out at the Institute of Physics, University of Tartu on two different setups, designed for experiments in UV-Vis (1.5–6 eV) and VUV (3–11 eV) excitation ranges:

- In the case of the UV-Vis setup, the luminescence characteristics were studied under excitation by UV light from a 400 W deuterium discharge lamp DDS-400 through a double-quartz prism monochromator DMR-4. The samples were mounted in a liquid helium cryostat (2–400 K) or in a Janis VPF-800 liquid nitrogen cryostat (78–800 K) by the means of conductive silver glue or a specially designed spring-equipped copper finger. Emission spectra were measured by using an ARC Spectra Pro 308i Czerny–Turner type grating monochromator equipped with a Princeton Instruments CCD (charge-coupled device) camera or with a second double-quartz prism monochromator DMR-4 equipped with a Hamamatsu H6240-01 photon counting head. Emission and excitation spectra were measured in the

temperature intervals 4.2–295 and 295–700 K, which was controlled with a LakeShore 331 or 335 temperature controller. Various colour glass filters, provided by SCHOTT or UQG Optics, were used in order to suppress the effects of second orders of excitation or emission and stray light. The experiment was fully controlled using a LabView based software.

- For the excitation in the region 3–11 eV, a vacuum system based on a VUV light source, a 200 W Heraeus deuterium discharge lamp, and a Seya-Namioka McPherson 234/302 monochromator equipped with a 300g/mm grating (spectral resolution 0.4 nm, dispersion 16 nm/mm, optimization for 140 nm) was used. The samples were mounted on the sample holder and placed in a closed-cycle helium cryostat provided by ARS (Advanced Research System, Inc.). The excitation source, primary monochromator and cryostat were connected to a vacuum system and the high vacuum 7×10^{-7} mbar was created with a turbo-molecular pump. The emission energy in the range 1–6 eV was selected by the means of an Andor SR 303i-B grating monochromator equipped with a CCD (Andor iDus 416) or with various photomultiplier tubes (H8259, H8259-01, H8259-02). All measurements were carried out in the temperature range 5–300 K and controlled by using a LabView based software.

The synchrotron radiation (SR) studies were conducted at two large scale facilities: at the SUPERLUMI station of the DORIS III storage ring (HASY-LAB, DESY, Hamburg, Germany), and at the undulator beamline I3 of the MAX-III storage ring in MAX IV Laboratory (Lund, Sweden):

- The SUPERLUMI station of HASYLAB has been described in details elsewhere [69]. The excitation and reflectivity spectra of various samples were measured in the energy region 4–20 eV, whereas the advantage of the natural polarization of the synchrotron radiation in the horizontal plane was taken in the case of the study of oriented crystals. The reflectivity spectra were measured in near normal incidence (angle 17°) geometry. The luminescence was analysed with a SpectraPro308i (Acton) spectrograph and a Hamamatsu PMT R6358P.
- The SR studies at MAX-III storage ring were carried out by the means of the mobile luminescence endstation installed on the FINEST branch of the I3 beamline (for more details see [70, 71]). The excitation energy was varied by the means of a 450 lines/mm Au grating (suitable for energies 5–50 eV) with a 6.65 m off-plane Eagle primary monochromator. Both vertical and horizontal polarizations were used in the case of measuring excitation spectra of oriented crystals. In order to suppress the second order of excitation, a LiF filter was used at excitation energies below 12 eV. For selecting the emission energy, a Czerny-Turner type ARC SpectraPro 300i grating monochromator was used. The emission signal was collected by a fibre optic system and delivered to the monochromator. The signal detection was carried out with a Hamamatsu H8259-01 photomultiplier tube. The endstation was equipped with a helium-flow cryostat allowing a temperature range of 7–320 K.

At both setups, the excitation spectra were normalized to the reference signal of sodium salicylate to equalize the quantum intensities of the synchrotron radiation falling onto the crystal at different photon energies. The emission spectra were corrected for the monochromator spectral efficiency and spectral sensitivity of the detector.

3.2.2. Radioluminescence and cathodoluminescence

An external X-ray device URS-01 (Cu anode, 20 kV, 0.4 mA) was used for the excitation of a sample mounted on a crystal holder and placed in a helium bath cryostat. The irradiation of the samples was carried out through the beryllium window of a liquid helium cryostat at 4.2 K.

All cathodoluminescence studies were carried out at the custom-made two-channel setup equipped with a helium bath cryostat, which allowed the luminescence registration at temperatures 5–400 K. The combination of the short-wavelength channel (4–11 eV) based on a Johnson-Onaka double monochromator (equipped with Hamamatsu PMT R6836) and the long-wavelength channel (1.8–6 eV) based on an ARC SpectraPro 2300i grating monochromator equipped with various detectors, enabled to cover the luminescence spectral range from VUV to NIR. In this setup, excitation is carried out with an electron gun (Kimball Physics EGG-3101) with energies up to 10 keV, which can be used both in steady and pulse (10 ns, 5 kHz) modes. An electron beam was focused on the surface of the sample into a spot of about 0.5 mm², with the penetration depth around 0.5 μm. After irradiation with electrons in steady mode, it is also possible to register phosphorescence or thermostimulated luminescence, spectrally integrated in the region of 1.8–6 eV or at selected emission energy in each channel. The TSL curves were measured with a heating rate of 10 K/min. The setup is described in more detail in [72, 73].

In the case of oriented and polished single crystal samples of differently doped Li₂B₄O₇, the problem of surface charging aroused. The redundant charge on the surface of dielectric samples causes pyroelectric buildup that may result in appearance of false bands or peaks in spectra or glow curves, respectively. To avoid or at least suppress surface charging under electron beam excitation, the 5-nm thick Pt or Au films were deposited on all crystal samples.

3.2.3. Thermostimulated luminescence

The TSL spectra and glow curves were measured on three different custom made setups in the region 5–700 K. The first one exploiting electron gun as an irradiation source, has been already specified in the previous chapter.

In the case of the second setup, samples were irradiated with an X-ray tube (W anode, 50 kV, 15 mA) at room temperature and then mounted in a Janis VPF-800 cryostat. The integral TSL curves were measured at a heating rate of

10 K/min in the temperature intervals 295–700 K, controlled with a LakeShore 335 temperature controller and recorded using a Hamamatsu H8259-02 photon counting head. If necessary, a neutral glass filter NS-13, Russia, was placed in front of H8259-02 to reduce the integral intensity. The TSL emission spectra were repeatedly measured in 30 s intervals within each TSL peak using an ARC SpectraPro 308i grating monochromator equipped with a CCD detector with spectral sensitivity in the range 190–1100 nm. In some case, the spectra were registered with a double-quartz prism monochromator DMR-4 equipped with a Hamamatsu H6240-01 photon counting head. Considering the given heating rate, each spectrum was measured within a temperature interval of 5 K. All measurements were fully controlled using a LabVIEW based software.

In the case of the third setup, the samples were irradiated with a metrological class ^{239}Pu source (6.02×10^5 α -particles/s with a dose rate 1.23 mGy/s, for a 4.5 mm sample), and then the integral TSL curves were recorded in the temperature interval 290–685 K with a custom-made TL reader based on a computer-controlled thermocontroller OMRON E5CK and PMT FEU-79, with a typical heating rate 20 K/min.

At temperatures above 500 K an increasing near-infrared emission emanating from the heater and the sample holder of the cryostat started affecting the shape of the TSL glow curve. In some cases, at considerably higher temperatures, this deep-red emission could even exceed the luminescence originating from the sample. For that reason, a TSL curve was recorded from irradiated samples, and after cooling the sample down to room temperature, the measurement was repeated in the same configuration on the same sample, yielding this way a heat background correction curve. The TSL glow curve was corrected by subtracting the background signal from the primary glow curve.

3.2.4. Electron paramagnetic resonance study

The electron paramagnetic resonance (EPR) studies were carried out at the Institute of Physics, University of Tartu, Estonia and at the Institute of Physics of the Czech Academy of Sciences, Prague, Czech Republic.

In the former case, the EPR studies were performed with an X-band spectrometer RE 1301, Russia, possessing a 975 kHz frequency of magnetic field modulation, at 77 K and RT. Before EPR measurement the samples were irradiated with an X-ray tube (W-anode, 53 kV, 14 mA). The step annealing of EPR signal was carried out to a certain temperature point. After reaching the temperature point, the sample was removed from the heater plate, and the EPR signal was recorded.

The second EPR setup was based on a Bruker X-/Q-band E580 FT/CW ELEXSYS spectrometer at X-/Q-band with the microwave frequencies 9.3–9.5 GHz and 33–44 GHz, respectively. An X-ray tube (W anode, 55 kV, 30 mA) was used for the irradiation of the samples. EPR spectra were taken at room temperature.

4. RESULTS AND DISCUSSION

4.1. Spectral characteristics of impurity ions and their position in lattice

4.1.1. $\text{Li}_2\text{B}_4\text{O}_7\text{:Cu}$

For the purpose of further comparison with TSL properties in irradiated samples, here we show most relevant features of the LTB:Cu emission based mainly on the results of ref. [45]. The emission spectrum of LTB:Cu crystal at 10 K is dominated by a strong and relatively narrow band peaking at 370 nm (3.35 eV) (Fig. 2, curve 2) appreciably differing from the emission spectra of STEs recorded from undoped LTB crystals (curve 1). Despite the strong overlap between the 3.35 eV and STE emission they can be easily distinguished by substantially smaller half-width of the 3.35 eV emission band. This emission has been related to Cu^+ ions in earlier papers [74, 75, 76]. The excitation spectra recorded for the 3.35 eV emission for two orientations of the electric vector of the exciting light with respect to the crystal axes, $E \parallel c$ and $E \parallel b$, are presented in Fig 2 (curves 2' and 2'', respectively). They consist of two main band groups whose shape and intensity ratio depends on exciting light polarization.

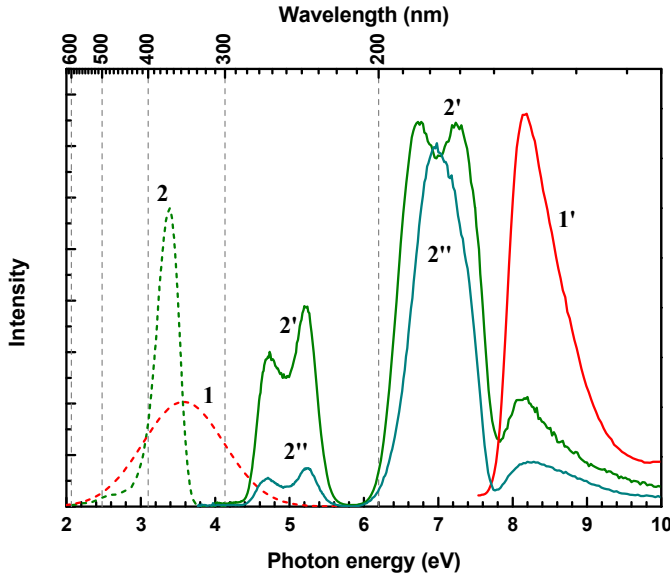


Fig. 2. Emission spectra of $\text{Li}_2\text{B}_4\text{O}_7$ (1) and $\text{Li}_2\text{B}_4\text{O}_7\text{:Cu}$ (2) crystals excited at 8.5 and 5.3 eV, respectively, and the excitation spectra recorded for the 3.65 (1') and 3.35 eV (2', 2'') emissions at 10 K. The excitation spectra (2' and 2'') were recorded for the $\text{Li}_2\text{B}_4\text{O}_7\text{:Cu}$ crystal for two different polarizations of the exciting light, $E \parallel c$ (2') and $E \parallel b$ (2'').

Two peaks at 4.75 and 5.2 eV are observed for the low-energy group at both orientations, while the high-energy group is represented by two peaks at 6.8 and 7.20 eV for $E\parallel c$ and only one band peaking at 7 eV for $E\parallel b$. These two groups of excitation bands situated at 5 and 7 eV were ascribed to the $3d^{10} \rightarrow 3d^9 4s$ and $3d^{10} \rightarrow 3d^9 4p$ transitions, respectively. Copper impurity has been found in two valence states, Cu^{2+} and Cu^+ , both substituting for Li^+ ions [45, 77].

4.1.2. $\text{Li}_2\text{B}_4\text{O}_7\text{:Ag}$

The emission spectra of $\text{Li}_2\text{B}_4\text{O}_7\text{:Ag}$ crystals at low temperatures 5–10 K are dominated by the band peaking at 268 nm (4.62 eV) (Fig. 3, curve 1). Such emission has been tentatively ascribed to Ag^+ ions in earlier papers [51–53]. In order to identify the involved electronic states more reliably, we recorded the excitation spectra of the impurity-related 4.62 eV emission band for oriented $\text{Li}_2\text{B}_4\text{O}_7\text{:Ag}$ crystals in a wide energy region from 5 to 20 eV and compared them with calculated density function spectra of an Ag^+ impurity placed in a Li^+ site in the $\text{Li}_2\text{B}_4\text{O}_7$ matrix. The excitation spectra for two orientations of the electric vector of the exciting light with respect to the crystal axes ($E\parallel c$ and $E\parallel b$)

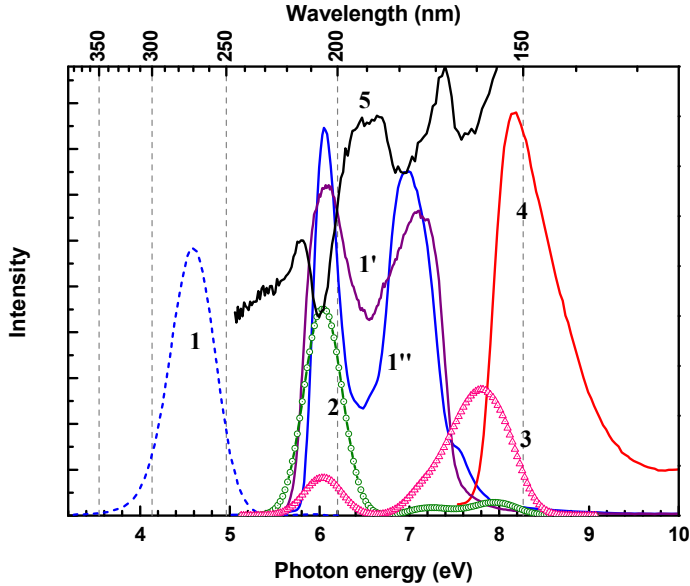


Fig. 3. Ag^+ emission spectrum for $E_{\text{exc}}=6.05$ eV (1), excitation spectra of the 4.62 eV emission for the exciting light polarisation $E\parallel c$ (1') and $E\parallel b$ (1'') and reflectivity spectrum measured for $E\parallel b$ (5) in $\text{Li}_2\text{B}_4\text{O}_7\text{:Ag}$ at 9 K. For comparison, the excitation spectrum of the STE emission at 3.65 eV in an undoped crystal is given (4). Curves 2 and 3 represent the calculated density function of the $5s$ and $5p$ excited states of Ag^+ , respectively.

are shown in Fig. 3, curves 1' and 1'', respectively. The spectrum measured for *E*||*b* consists of three non-elementary bands peaking near 6.05, 7.05 and 7.7 eV, the latter being substantially distorted due to the host lattice absorption. To give an estimate of the position of the fundamental absorption edge, the excitation spectrum of the excitonic emission is shown in the same figure (curve 4). There is a strong overlap between the excitation spectra of the excitonic and impurity emissions, at least in the 7.5–8 eV region. The presence of three impurity-related absorption bands at the above listed positions is demonstrated also by the reflectivity spectrum for the exciting light polarisation *E*||*b* (Fig. 3, curve 5). The crystal reflectivity, gradually decreasing in the transparency region toward longer wavelengths as expected, demonstrates clear dips at the positions of the impurity absorption bands near 6.05 and 7.05 eV. A similar dip is recorded also near 7.7 eV, which testifies the influence of strong impurity absorption even though the host absorption is already rather strong at this energy. These reflectivity dips appear in the transparency region of the crystal due to the absorption of the light reflected from the rear surface of the sample by impurity ions. No direct absorption measurements were performed in the VUV region for this crystal. It is worth noting that the excitation spectra of the 4.62 eV emission measured for *E*||*b* and *E*||*c* possess clearly different structural details revealing a strong anisotropy of the splitting of the degenerated electronic states of the impurity ion at the lattice site occupied.

The above data are sufficient for the comparison with the results of *ab-initio* calculations allowing the identifications of the luminescence centre responsible for the 4.62 eV emission. The calculations were performed under the plausible supposition based on general physicochemical consideration and literature data that the 4.62 eV emission originates from the $4d^9 5s \rightarrow 4d^{10}$ transition of an Ag^+ ion substituted for Li^+ . The density functions of the 5s and 5p excited states calculated for the Ag^+ impurity in $\text{Li}_2\text{B}_4\text{O}_7$ by using CASTEP module [78] of the Material Studio package are shown in Fig 3, curves 2 and 3, respectively. The generalized gradient approximation (GGA) [79] was used to treat the correlations effects. The plane waves cut-off energy was 300 eV, the k-points grid was chosen as $2 \times 2 \times 2$. The convergence criteria were 2.0×10^{-5} eV/atom for total energy, 0.05 eV/Å for the maximal force, and 0.002 Å for the maximal displacement. The calculations were performed for a model cluster consisting of one unit cell of $\text{Li}_2\text{B}_4\text{O}_7$ where one out of eight Li^+ ions was replaced by an Ag^+ ion, assuming periodic boundary conditions. The concentration of the Ag^+ impurity is strongly exaggerated under such assumption, but the result should give correct relative positions of the Ag 5s and 5p states. A similar approach for the analysis of the impurity effects on the optical and electronic properties of the doped crystals was successfully employed in [80]. As the bandgap energy is usually underestimated in this kind of calculations, we adjusted the position of the first calculated peak to the maximum of the lowest energy excitation peak in the experimental spectrum. The scissor factor was taken 1.6 eV in this case. The calculation method used does not provide electronic transition probabilities, for that reason the calculated band ratio cannot be directly compared to that observed in the excitation spectra.

Nevertheless, the relative positions of the maxima of the calculated density function coincide with good accuracy with those observed in the excitation spectrum of the 4.62 eV emission. This is a strong argument in favour of ascribing the 4.62 eV emission to the electronic transition of Ag^+ ions occupying a Li^+ site. The more complicated structure that is distinctly recognised in the experimental excitation spectrum for the case of *E*1*c* (Fig. 3, curve 1') may rise from the spin-orbit and low-symmetry splitting of the $5p$ states of the Ag^+ ions. Thus, the presence of Ag^+ in $\text{Li}_2\text{B}_4\text{O}_7:\text{Ag}$ crystals is theoretically verified.

4.1.3. $\text{Li}_2\text{B}_4\text{O}_7:\text{Cu,Ag}$

Emissions of both Ag^+ and Cu^+ ions were observed in $\text{LTB}:\text{Cu,Ag}$ crystals (Fig. 4). No new emission or excitation bands were found with respect to those known for $\text{LTB}:\text{Cu}$ and $\text{LTB}:\text{Ag}$. The emission of Ag^+ centers at 4.62 eV overlaps with the lowest-energy component of the absorption band near 4.7 eV of Cu^+ centers (Fig. 4, curves 2, 1'). For that reason, one could expect Ag^+ to play a sensitizer role for Cu^+ emission as has been suggested also in [53, 55]. The energy transfer from Ag^+ to Cu^+ in $\text{LTB}:\text{Cu,Ag}$ crystals is clearly demonstrated by the presence of the Ag^+ related shoulder at 6.1 eV in the excitation spectrum of Cu^+ emission (Fig. 4, curve 1'). This effect is certainly important under X-ray irradiation due to the shift of the crystal emission to the low-energy side more suitable for detection.

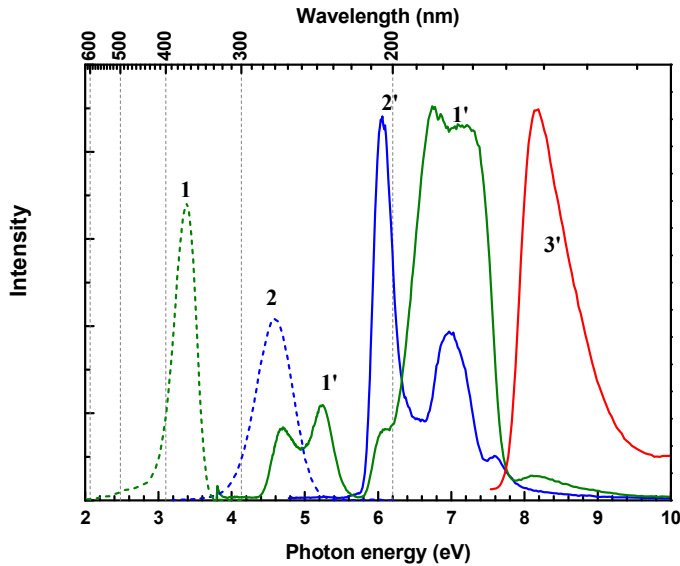


Fig. 4. Emission spectrum of Cu^+ at $E_{\text{exc}}=7$ eV (1) and Ag^+ at $E_{\text{exc}}=6.05$ eV (2), and corresponding excitation spectra for $E_{\text{em}}=3.35$ (1') and $E_{\text{em}}=4.62$ eV (2') measured for *E*1*b* in $\text{Li}_2\text{B}_4\text{O}_7:\text{Cu,Ag}$ at 9 K. The excitation spectrum of the STE emission at 3.65 eV in an undoped crystal is also presented (3').

4.1.4. $\text{Li}_2\text{B}_4\text{O}_7\text{:Mn}$ crystals and ceramics

The emission spectra of the studied $\text{Li}_2\text{B}_4\text{O}_7\text{:Mn}$ crystals and ceramics excited in the spectral range from visible (2.5 eV) to vacuum ultraviolet (VUV, <8 eV) at 5 K were dominated by the band peaking at 608 nm (2.03 eV) (Fig. 5, curve 1). In addition, a weak green luminescence peaking at 550 nm (2.25 eV) could be also observed under excitation in the region 2.5-3.5 eV. A combined excitation spectrum of the 2.03 eV emission band is presented in Fig. 5a (curves 1' - 3', 3'') for $\text{Li}_2\text{B}_4\text{O}_7\text{:Mn}$ crystals and Fig. 5b (curves 1', 2' - 2''') for ceramics $\text{Li}_2\text{B}_4\text{O}_7\text{:Mn}$.

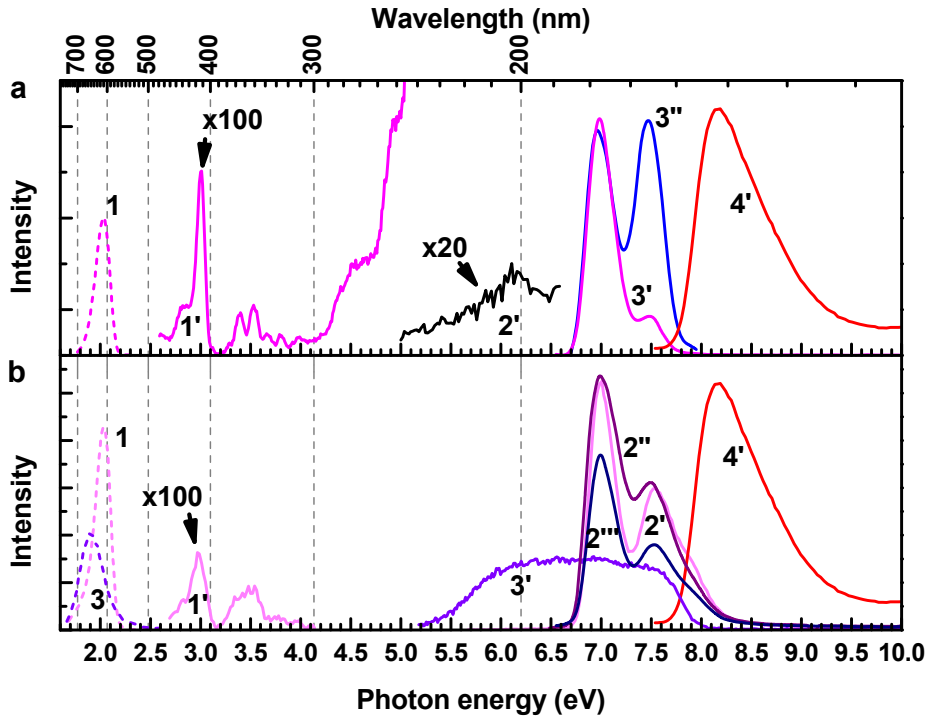


Fig. 5. a) Emission (1) and excitation (1'-4', 3'') spectra measured at different setups (see text for more details) for a $\text{Li}_2\text{B}_4\text{O}_7\text{:Mn}$ crystal. Curves 3' and 3'' were measured for two different orientations of the electric vector of exciting light with respect to the c axis of the crystal, $E \parallel c$ (3'') and $E \perp c$ (3'). Curve 4' – excitation spectrum of the STE emission at 3.65 eV. **b)** Emission spectrum at $E_{exc}=7$ eV (1), the excitation spectrum of the $E_{em}=2.03$ eV emission (1', 2' - 2''') of a $\text{Li}_2\text{B}_4\text{O}_7\text{:Mn}$ (0.13 mol%, MnCO_3) (1', 2'), $\text{Li}_2\text{B}_4\text{O}_7\text{:Mn}$ (0.25 mol%, KMnO_4 – point defects) (2''), $\text{Li}_2\text{B}_4\text{O}_7\text{:Mn}$ (0.25 mol%, KMnO_4 – aggregates) (2'''), respectively. The excitation spectrum measured for the STE emission of a $\text{Li}_2\text{B}_4\text{O}_7\text{:Mn}$ (0.13 mol%, MnCO_3) ceramic (4'). Emission spectrum at $E_{exc}=6.4$ eV (3) and excitation spectrum of the 1.92 eV emission (3') of a $\text{Li}_2\text{B}_4\text{O}_7\text{:Be}$ (0.13 mol%), Mn (0.13 mol%) sample. $T=9$ K.

Due to a strong variation of the excitation efficiency over the studied energy range, the spectra were recorded with three different setups: with a double-quartz prism monochromator in the range 2.5–6 eV, with a McPherson 234/302 grating monochromator in the range 5–9 eV, and at the I3 undulator beamline of the MAX-III synchrotron ring in the range 5.5–20 eV. Different parts of the spectra were stitched together and their relative intensities estimated using the regions of most reliable overlapping. The magnification coefficients for different parts of the excitation spectra are shown in Fig. 5a and 5b. Besides that separate transitions are better resolved in our spectra, the general appearance of the spectrum in the range of 2.5–6 eV (Fig. 5a) is similar to those observed earlier [52, 67]. It is generally accepted that the emission band at 2.03 eV is connected with the ${}^4T_1({}^4G) \rightarrow {}^6A_1(S)$ transitions within the $3d^5$ configuration of the Mn^{2+} ions. Due to well-resolved spectra we were able to ascribe various peaks in visible-to-UV region to certain transitions within the same electronic configuration according to the Tanabe-Sugano diagram (see Table 2).

Two excitation spectra of the 2.03 eV emission were measured in the region 5.5–20 eV for oriented $Li_2B_4O_7:Mn$ samples with two different orientations of the electric vector of exciting light with respect to the c axis of the crystal, $E \parallel c$ and $E \perp c$ (Fig. 5a, curves 3'' and 3', respectively). The spectra in the VUV region are represented by doublet of two well-resolved bands at 7.0 and 7.5 eV with comparable half-widths and the intensities equal in the case of $E \parallel c$ but substantially different for $E \perp c$. A high-energy slope of the peak at 7.5 eV is distorted due to the influence of the fundamental absorption edge close to 8 eV. The position of the latter is represented in Fig. 5a and b, curve 4' by the onsite of the excitation spectrum of the self-trapped exciton in LTB. To the best of our knowledge, the excitation spectra of the $Li_2B_4O_7:Mn$ crystals have not been earlier studied in the VUV region. The excitation spectra of the 2.03 eV band possess a well-resolved structure which allows suggesting that Mn^{2+} ions responsible for the emission occupy well-defined positions in the lattice site. On the contrary, in the LTB:Be(0.13 mol%),Mn(0.13 mol%) ceramics, in which the co-doping by Be is supposed to facilitate the aggregation of Mn^{2+} in clusters, the excitation spectrum of red-shifted emission peaking at 1.92 eV (Fig. 5b, curve 3) is represented by a broad structureless band covering the whole region between 5 and 8 eV (curve 3'). One can suggest that this shifted emission originates from a family of complex Mn^{2+} centres with various structures possibly situated at irregular sites or grain boundaries. The traces of the same emission may be responsible for a slight asymmetry of the main 2.03 eV emission on the long wavelength side observed in LTB:Mn ceramics.

The oscillator strengths of the transitions within the $3d^5$ configuration of the Mn^{2+} ions in the region 2.5–5.5 eV are very small due to the spin forbiddance, and the corresponding luminescence is very weak in our experiments. On the contrary, the excitation efficiency of the 2.03-eV luminescence in the VUV region is very high, exceeding that in the visible region by two orders of magnitude. This allows one to suggest that the doublet at 7.0 and 7.5 eV corresponds to spin-allowed transitions and is most likely related to the

$3d^5 \rightarrow 3d^4 4s$ transitions populating the 6D term split by crystal field in two sub-bands [81]. A similar doublet has been also recorded in another wide-gap material, KMgF_3 [82].

Thus, the excitation spectrum of the 2.03 eV emission is characterized by well-resolved narrow bands in the visible-UV region and strong narrow bands in the VUV region demonstrating a remarkable dependence on crystal orientation, i. e. on exciting light polarisation. As the splitting of the 6D term is expected to strongly depend on crystal field, this indicates that spectroscopically active Mn^{2+} ions responsible for this emission are located in lattice sites of essentially one given type. We suppose that weakly defined interstitial positions of Mn^{2+} ions may be excluded in view of the strong polarisation effects observed for the $3d^5 \rightarrow 3d^4 4s$ transitions, in accordance with the EPR results below. It can also be concluded that the contribution of aggregated centres is marginal primarily because of the observation of narrow excitation bands in the VUV spectral region. For example, this part of the spectrum looked structureless in LTB:Mn ceramics co-doped by Be (Fig. 5b, curve 3'), which facilitated aggregation of the Mn^{2+} in the lattice.

Table 2. The d-d transitions of Mn^{2+} in octahedral symmetry for $\text{Li}_2\text{B}_4\text{O}_7\text{:Mn}$, assigned on the basis of the Tanabe-Sugano diagram for the transitions from the ground level 6A_1 .

Identified transition	Photon energy (eV)
${}^6A_1(\text{S}) \rightarrow {}^4T_1(\text{G})$	2.53
${}^6A_1(\text{S}) \rightarrow {}^4T_2(\text{G})$	2.85
${}^6A_1(\text{S}) \rightarrow {}^4A_1(\text{G}), {}^4E(\text{G})$	3.01
${}^6A_1(\text{S}) \rightarrow {}^4T_2(\text{D})$	3.40
${}^6A_1(\text{S}) \rightarrow {}^4E(\text{D})$	3.53
${}^6A_1(\text{S}) \rightarrow {}^4T_1(\text{P})$	3.66 3.78
${}^6A_1(\text{S}) \rightarrow {}^4A_2(\text{F})$	4.62
${}^6A_1(\text{S}) \rightarrow {}^4T_1(\text{G}) + {}^4A_1(\text{G}); {}^4E(\text{G})$	4.98
${}^6A_1(\text{S}) \rightarrow {}^2A(\text{H})$ ${}^6A_1(\text{S}) \rightarrow {}^2A(\text{G2})$	6.1

The available spectra provide controversial information about the coordination of Mn^{2+} in the LTB crystals studied. On the one hand, the crystal field splitting of the 6D term is of the order of $10Dq \approx 4000 \text{ cm}^{-1}$ (Fig 5a, curve 3''), indicating $Dq \approx 400 \text{ cm}^{-1}$ characteristic of materials with tetrahedrally coordinated Mn^{2+} ions [83]. For octahedral coordination the splitting should be at least twice as large [84–86]. On the other hand, there are indications in the literature that Mn^{2+} ions have emission bands in the region of 500–550 nm for tetrahedral coordination and in the region of 600–650 nm for octahedral

coordination [87]. In both configurations, the ${}^4T_1({}^4G)$ is the lowest excited level responsible for the emission (compare, e.g., [83] and [88]), the interaction with ligands defining only its energy position. Contrary to the expectations prompted by the low Dq value, in our LTB:Mn crystals the emission band of the Mn^{2+} ion is centred at 608 nm (2.03 eV), rather indicating an octahedral coordination of the ion. A photoexcited emission band of Mn^{2+} ions has been observed also at 527 nm in a LTB:Mn powder, however, the TSL spectrum was still peaked at about 600 nm in that material [3]. These facts indicate a relaxation of the Mn^{2+} ion inside of its strongly distorted, tetrahedral-octahedral oxygen cage, occurring not only upon thermal treatment or amorphisation, but also upon electronic excitation. Such a behaviour corresponds to the crystallographically weakly defined Li site and the resulting instable character of the whole Li sublattice (see [33, 87] and references therein) responsible for peculiarities in a series of phenomena including TSL to be discussed later.

We also measured the emission and excitation spectra for the crystals irradiated by X-rays with the dose of 18 kGy and obtained important result that the emission band position of the irradiated sample remained the same (2.03 eV), with no change of its excitation spectrum either, while the total intensity decreased by factor of three. This fact suggests recharging processes involving Mn^{2+} ions in $Li_2B_4O_7:Mn$ crystals under irradiation, in good agreement with the below-treated EPR results and conclusion made in Ref. [67].

The above-described spectroscopic characteristics of undoped as well as Cu, Ag, and Mn doped LTB crystals provide a reliable basis for the interpretation of emission spectra measured under excitation by ionizing radiation or during recombination processes following irradiation. As shown below the comparison helps to assess the role of the STE and impurity ions in recombination luminescence, luminescence center formation, charge trapping, and energy storage processes taking place in crystals exposed to ionizing radiation.

4.1.5. Mn^{2+} ions localization in the $Li_2B_4O_7$ lattice

EPR spectra of Mn^{2+} measured in the X band are difficult to analyze as the zero field splitting is comparable to the X-band quantum energy. For a better separation of the Mn^{2+} transitions, measurements in the present study were mainly done in the Q band at 33.8 GHz. The RT spectra for two orientations of the external magnetic field \mathbf{B} in the (ac) rotational plane are shown in Fig. 6; the upper spectrum corresponds to an angle of 45° with the crystallographic axis \mathbf{a} (where the spectrum is the broadest) and the lower one to $\mathbf{B} \parallel \mathbf{a}$.

The upper spectrum is characterized by eight clearly discernible groups of intense resonance lines. One of these groups, labeled “7” and indicated by a bracket is demonstrated in the zoomed inset of Fig. 6 to consist of four superposed sextets indicated by colored vertical markings. The resonance lines within each sextet are separated by approximately 80 G. The spectra in Fig. 6 are centred on a g value near 2 (magnetic field ~ 12.1 kG). Those are common

features of EPR spectra originating from single Mn^{2+} ions ($3d^5$ outer shell with electron spin $S = 5/2$) with the ^{55}Mn nucleus having nuclear spin $I = 5/2$ and 100% abundance [89, 90]. Since in the Q-band the Zeeman interaction is markedly larger than the crystal field splitting, all five transitions expected for $S=5/2$ can be located though not fully distinguished in the central parts of the spectrum (see caption of Fig. 6). Taking into account also the hyperfine (HF) splitting due to the ^{55}Mn nuclear spin, there are $5 \times 6 \times 8 = 240$ spectral lines for an arbitrary direction of the magnetic field (related to only the allowed transitions) which originate from eight magnetically inequivalent families of Mn^{2+} centres. In reality, the number of spectral lines in the spectrum is much larger due to forbidden transitions which, however, have smaller intensities than the allowed ones.

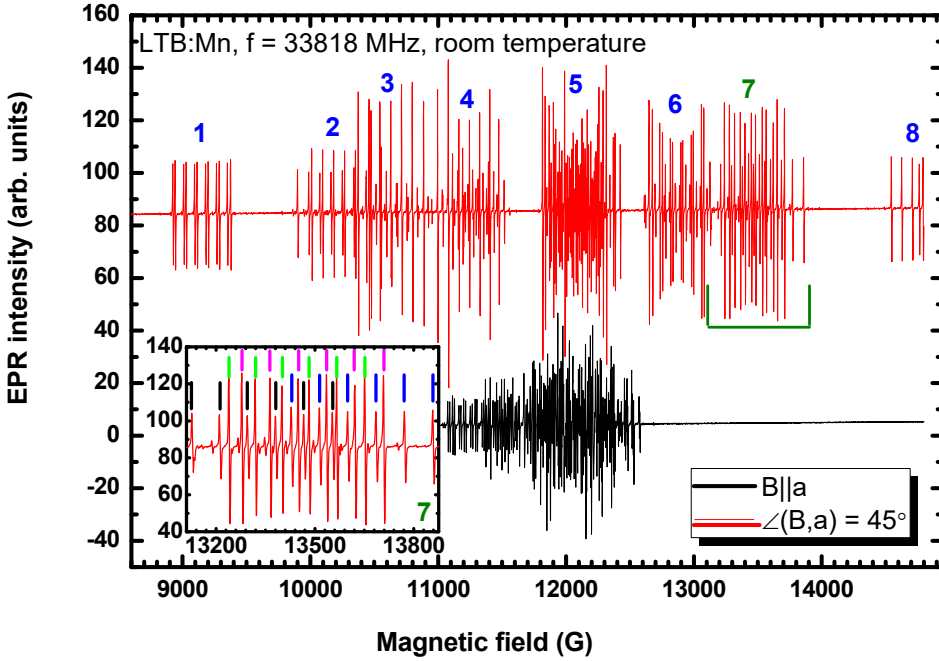


Fig. 6. EPR spectra of Mn^{2+} ions in $\text{Li}_2\text{B}_4\text{O}_7:\text{Mn}$ measured for two orientations of the external magnetic field in the (ac) rotational plane. The inset zooms the spectral part 7 (indicated by a bracket) consisting of four superposed sextets (see markings in different colours) each being a characteristic six-line hyperfine structure (HFS) common for the ^{55}Mn isotope. Numbers 1–8 indicate discernible groups of resonance lines each corresponding to several superposed electron spin transitions of the fine structure as follows: 1,2 – two $5/2 \leftrightarrow 3/2$ transitions; 3,4 – two $3/2 \leftrightarrow 1/2$ transitions; 5 – four $1/2 \leftrightarrow -1/2$ transitions; 6 – two $1/2 \leftrightarrow -3/2$ transitions; 7 – two $1/2 \leftrightarrow -3/2$ and two $-3/2 \leftrightarrow -5/2$ transitions; 8 – two $3/2 \leftrightarrow -5/2$ transitions.

To obtain information on the surroundings of the Mn^{2+} centres, angular dependences of the Mn^{2+} spectra were measured in the **(ab)** and **(ac)** rotational planes. The corresponding resonance fields as a function of rotation angle are presented in Fig. 7. Due to multiple overlaps, the determination of a complete set of spectral parameters is rather difficult, however, using the isotropic approximation for the g and HF tensor, acceptable for a $3d^5$ configuration, the isotropic values of these, together with fair estimates of the main crystal field parameters can be derived [33, 91].

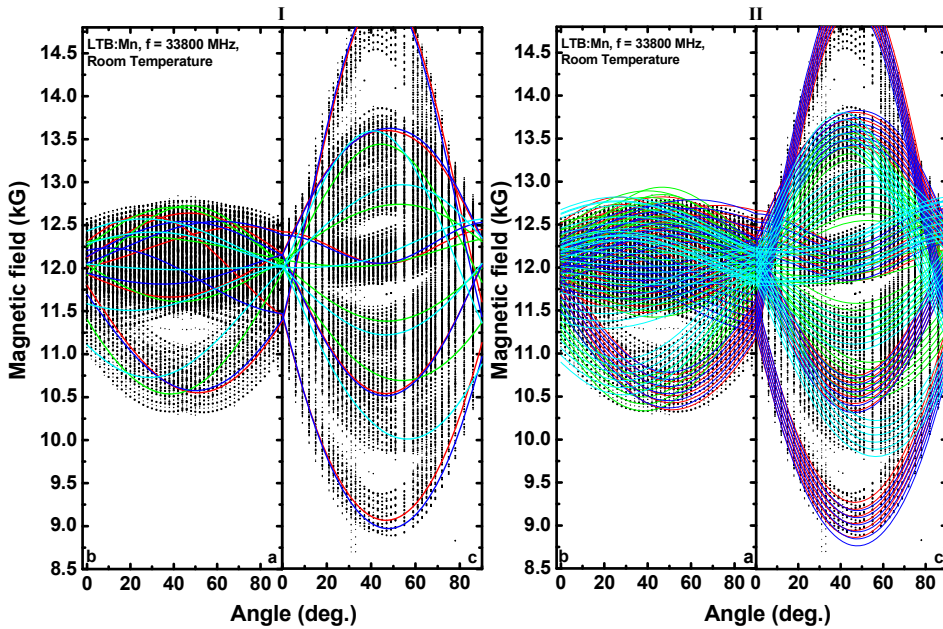


Fig. 7. Angular dependences of the Mn^{2+} resonance line positions (dots) and their fitted values (solid lines) representing: **I**) fine transitions only (centres of gravity of the ^{55}Mn sextets) and **II**) the calculated curves with the ^{55}Mn hyperfine structure. The lines are distinguished by color to show the contributions from four discernible magnetically inequivalent centre orientations. Dot size is proportional to spectral line intensity.

Before proceeding to a quantitative analysis, basic qualitative information can be extracted from the symmetry and the extremal positions of the angular dependences in Fig. 7, reflecting structural properties of the crystal and the paramagnetic defect, respectively. Due to the C_{4v} point group symmetry (tetragonal space group $I4_1cd$) of the LTB lattice [33] eight magnetically inequivalent centre families should be considered for a single type of paramagnetic centre of C_1 symmetry, reducing to four if the magnetic field is in the crystallographic plane **(ab)** or **(ac)**. Accordingly, to fit the angular dependences in Fig. 7 four sets of fitting curves for each rotational plane are needed, while

the small additional double splitting of the resonance lines (visible in Fig. 6) can be attributed to the misalignment of the small samples. On the other hand, this shows indeed the presence of eight magnetically inequivalent Mn^{2+} positions.

The mirror symmetry of the experimental points in the **(ab)** panel of Fig. 7 corresponds to $[110]$ type glide planes in the LTB structure. Two B_4O_7 units connected by such a symmetry element are seen on the left-hand side of Fig. 8a showing an **(ab)** projection of the crystal structure [33]. Similar units of exact C_2 symmetry, each containing two trigonally and two tetragonally coordinated boron sites, usually called B1 and B2 sites, form the covalent network of the LTB lattice (see Fig. 8a,b). The B1 and B2 sites by themselves have only approximate local threefold and tetrahedral symmetries with the main axes tilted by angles of $\sim 30^\circ$ and $\sim 10^\circ$ from the crystal C_2 symmetry axis, respectively. Taking into account the rigidity of the covalent network and the weakly distorted coordination of these sites, the local crystal potential seen by dopants substituted at one of these sites is also expected to reflect the approximate symmetry of the site. This should lead to extremal positions in the angular dependence of the outermost EPR lines if the direction of the magnetic field comes close to that of the approximate main symmetry axis. However, in the **(ac)** rotation plane the minimum and maximum (outside the available range) field positions occur for an angle close to 45° . This eliminates both types of boron sites (the tetrahedral B2 site by a large margin), independent of the direction of the tilts (actually reflecting the elongated shape of the B_4O_7 units).

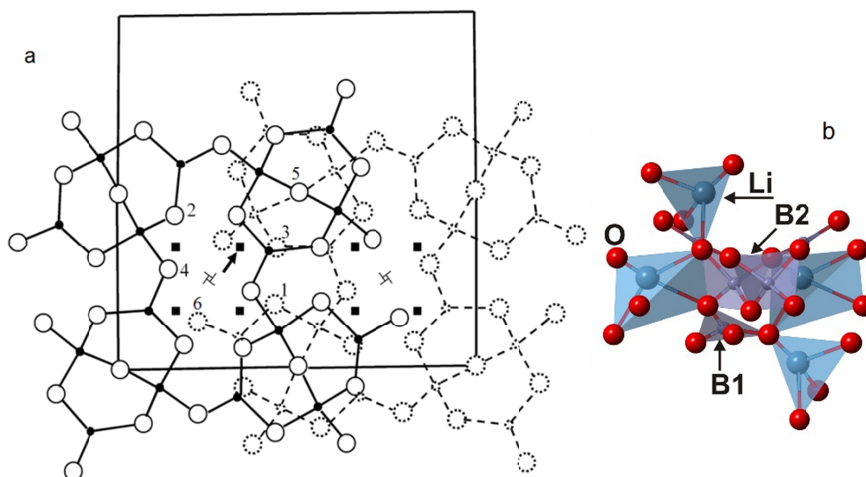


Fig. 8. a) Structure of the tetragonal elementary cell of LTB shown as a projection along the C_2 symmetry axis showing the -B-O-B- network and the Li sites located in the channels along the fourfold screw axes. The nearest oxygen neighbours of a chosen Li site (indicated by an arrow) are numbered [33, 45, 77]. **b)** A vertical (a,c) projection, showing the coordination of Li and the trigonal B1 and tetrahedral B2 sites of boron using data from [33].

Against Mn^{2+} substitution at or near a Li site there is no such argument as the six nearest oxygens in the surroundings of the Li site form a strongly distorted tetrahedron (four oxygens between 1.82 Å and 2.28 Å and two more at distances 2.55 Å and 2.76 Å (see Fig. 8a, for coordinates and more figures see Refs. [45, 77]). Relaxing the dopant inside this “octahedron” various coordinations from distorted tetrahedral to distorted octahedral can be obtained, which is also facilitated by the flexibility of the LTB lattice showing a series of thermal rearrangements in both undoped and doped LTB even below room temperature (see section 4.3).

Comparison of the Mn^{2+} ion with Cu^{2+} also substituting for Li^+ may give insight into possible differences of charge compensation and relaxation. While the Mn^{2+} ion has its strongest crystal field interaction along a direction making an angle of $\sim 45^\circ$ with the c axis, Cu^{2+} has its maximal g direction tilted by only $\sim 35^\circ$ from the c axis, together with a minimal g value along a $\sim [110]$ direction [45, 77]. Both cases seem to favour the presence of a nearest neighbour Li vacancy at an unrelaxed distance of ~ 3.1 Å within the same channel of easy movement of Li^+ ions (see Fig. 8a showing also the fourfold screw axes serving as winding staircases for the movement of Li^+ ions), while the differences indicate rather different relaxation for Mn^{2+} and Cu^{2+} which can be attributed to their different electronic configuration. For a $\text{M}^{2+}-\text{V}_{\text{Li}}$ complex within such a channel there are only two crystallographically different orientations (V_{Li} up or down the staircase) however, these may be energetically rather different, resulting in a single stable type of the complex.

Resonance fields were calculated using the “Easyspin 5.0.0 toolbox” program [92] considering the following spin Hamiltonian:

$$\hat{H} = \beta_e g \mathbf{S} \mathbf{B} + B_2^0 O_2^0 + B_2^{\pm 2} O_2^{\pm 2} + B_2^{\pm 1} O_2^{\pm 1} + A \mathbf{S} \mathbf{I}, \quad (1)$$

where β_e , g , A , \mathbf{S} , \mathbf{I} , \mathbf{B} are the Bohr magneton, g factor (taken isotropic for the $S = 5/2$), hyperfine constant, electron and nuclear spin operators, and magnetic field, respectively; $B_k^{\pm q}$, $O_k^{\pm q}$ ($q = 0, \pm 1, \pm 2$) are the zero field splitting constants and Stevens operators, respectively. Calculations were done assuming identical splitting constants for centre families related by mirror symmetry. The parameters determined from the fit are listed in Table 3 containing parameters for four centre families treated separately which essentially differ by magnetic axes orientation. Four other centres have practically identical parameters with those of the first quartet; the deviation in values is comparable with the accuracy of the spin-Hamiltonian parameter determination.

Table 3. Spin-Hamiltonian parameters of Mn^{2+} in the $\text{Li}_2\text{B}_4\text{O}_7$ lattice. Zero field parameters are given in 10^{-4} cm^{-1} . The accuracies of the parameter values are for g factor ± 0.005 , for A constant $\pm 0.5 \times 10^{-4} \text{ cm}^{-1}$ and for $B_k^{\pm q} \pm 5 \times 10^{-4} \text{ cm}^{-1}$.

No	Spin Hamiltonian parameters in the (abc) crystallographic frame						
	g	A	B_2^0	B_2^2	B_2^1	B_2^{-1}	B_2^{-2}
1	2.00	77	20.00	16.67	916.7	333.3	-126.7
2					383.3	716.7	-146.7
3					933.3	533.3	-86.7
4					500.0	1000.0	-40.0
	Spin Hamiltonian parameters in the (X,Y,Z) magnetic axes frame defined by the Euler angles α,β,γ						
	g	A	B_2^0	B_2^2	α	β	γ
1, 3	2.00	77	-285	135	35	46	0
2, 4			-285	135	58	46	0

The two values of α roughly add up to 90° as required for centres of different handedness in C_{4v} symmetry. Small discrepancies of the fit and the vanishing values of B_2^1 , B_2^{-1} and γ can be attributed to the neglect of higher order terms and of the difference between the two groups. The parameters determined within this thesis are unique as, to the best of our knowledge, only two papers [56, 66] contain EPR studies on LTB:Mn single crystals, performed only in the X-band without quantitative analysis due to indecipherable spectra in this band (see, e.g., spectra in section 4.1.7).

The sign of the B_2^0 constant was determined in a conventional way by comparing intensities of the $\pm 5/2 \leftrightarrow \pm 3/2$ transitions with decreasing temperature.

The satisfactory fit of the EPR spectra assuming the presence of only one type of centres suggests that Mn^{2+} ions are placed at only one site in the LTB lattice. The quantitative analysis yields spin-Hamiltonian parameters of the magnitude usual for Mn^{2+} centres in oxides and confirms the expectations about Li substitution.

Considerations about ionic radii are clearly in support of the Li site: Mn^{2+} ions with ionic radius exceeding several times those of boron in three- and fourfold oxygen coordination [93] might cause strong tensions in the lattice. On the other hand, rather close values of the ionic radii, 0.66 Å and 0.59 Å of Mn^{2+} and Li^+ for tetrahedral coordination [93], respectively, suggest that most probably Mn^{2+} is embedded at or near to a lithium site. Of course, it cannot be completely excluded that some Mn^{2+} ions are located at other lattice sites. However, their concentration should be at least one order of magnitude lower than those at Li sites. Otherwise, such Mn^{2+} ions could be distinguished in EPR spectra.

4.1.6. Comparison between crystal and ceramic $\text{Li}_2\text{B}_4\text{O}_7\text{:Mn}$

In order to compare crystal and ceramic LTB:Mn prepared by different techniques, both samples were ground into powder. The same amount of powder sample was used for EPR measurements. The spectra taken in the X-band are shown in Fig. 9.

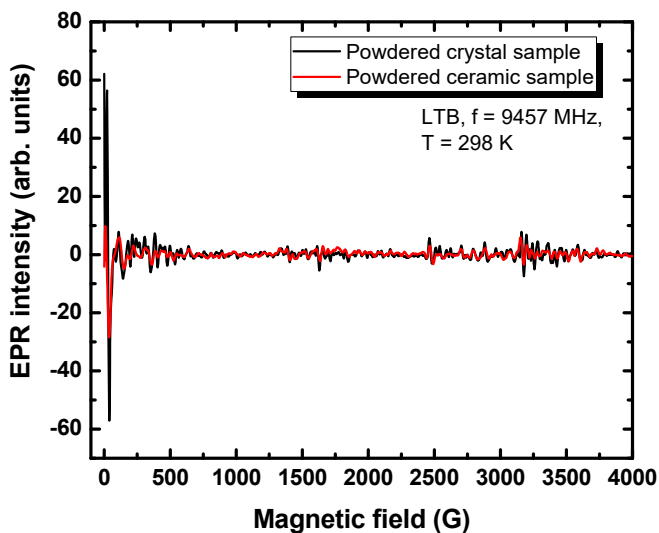


Fig. 9. X-band EPR spectra measured in crystal and ceramic $\text{Li}_2\text{B}_4\text{O}_7$ samples at RT.

It can be seen that the spectra in both ground crystal and ceramics are the same. Therefore, the Mn^{2+} ions can be assumed to occupy the same sites in both LTB ceramics and single crystals.

4.1.7. Influence of the X-ray irradiation

A single crystal sample has been irradiated by X-rays (55 kV, 30 mA) for 20 min at a 5 cm distance from the anode to the sample. EPR spectra taken before, immediately after, and one day after the X-ray irradiation are shown in Fig. 10.

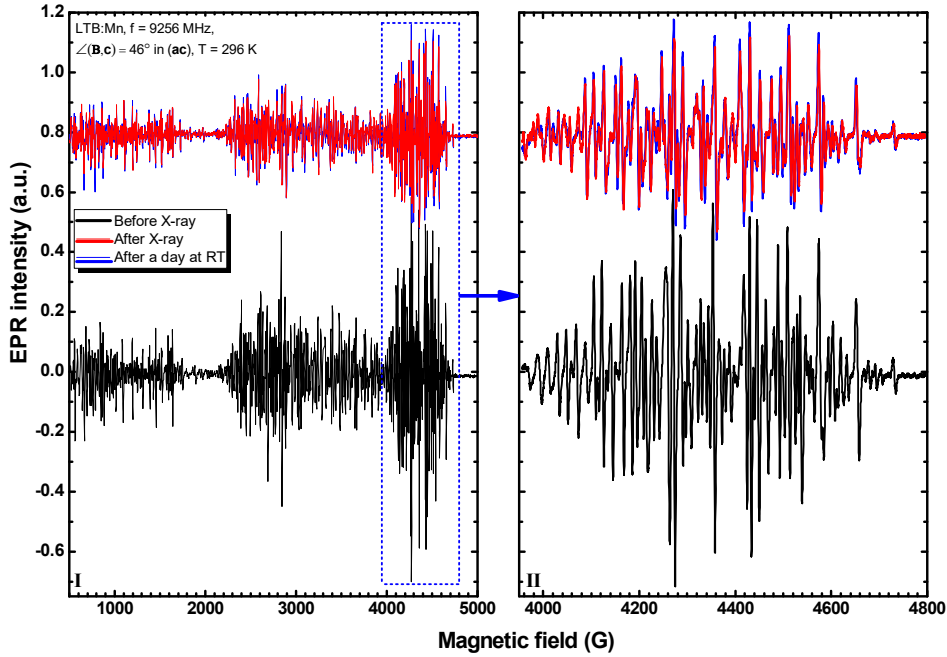


Fig. 10. EPR spectra measured in LTB:Mn before, immediately after and one day after X-ray irradiation. Panel II) shows an expanded spectral part from I).

One can see that irradiation essentially results only in a change of intensity (partial fading) and no other differences can be observed as seen very well in Fig. 10(II). This is another sign in favor of the Mn^{2+} to be found at one type of a lattice site as discussed above. Since the EPR intensity is directly proportional to the paramagnetic particle concentration, its decrease indicates recharging of the manganese ions from the paramagnetic Mn^{2+} to the EPR silent state of either Mn^+ or Mn^{3+} . However, this transformation is not fully conserved as after a day at room temperature, the intensity of the signal is partly restored (see Fig. 10). Note that the attempt to find Mn^+ or Mn^{3+} spectra by measurements down to the lowest temperature 3 K was unsuccessful, obviously due to the large zero-field splitting of energy levels of these non-Kramers ions.

4.2. Low temperature radioluminescence and cathodoluminescence of crystalline samples

The radioluminescence (RL) of undoped and copper doped $\text{Li}_2\text{B}_4\text{O}_7$ single crystals at 4.2 K are presented in Fig 11a, curves 1 and 2. In both cases the spectra consist of a broad structureless band centred at about 3.4 eV (365 nm) (see also [94]), which is similar but broader than the excitonic emission band (curve 4), and obviously comprises also perturbed exciton emissions originating

from recombination of charge carriers near defects. No direct indications for the relatively narrow Cu^+ luminescence band at 3.35 eV can be observed in the RL of the $\text{Li}_2\text{B}_4\text{O}_7:\text{Cu}$ crystal. The same is true also for cathodoluminescence of doped crystals (Fig. 11b). The CL spectra of $\text{Li}_2\text{B}_4\text{O}_7:\text{Cu}$ and $\text{Li}_2\text{B}_4\text{O}_7:\text{Ag}$ crystals measured at 5 K also consist of a broad structureless band peaking at 3.4 eV, whereas no impurity-related luminescence can be distinguished in either crystal (compare curves 1 and 2). Only in the case of $\text{Li}_2\text{B}_4\text{O}_7:\text{Mn}$, additional two substantially weaker bands peaking at 1.9 and 2.1 eV were observed. There is no major difference between the spectra measured under X-ray and electron excitation, apart from the larger intensity and slightly narrower shape of the CL spectra. The type of irradiation caused only minor variation also in the case of low-temperature TSL spectra to be treated in the following sections.

Supposedly, at low temperatures the main cathodoluminescence or radioluminescence mechanism is related to the recombination of conduction band electrons with holes trapped near cation vacancies or other intrinsic and extrinsic defects. This could explain the dominating perturbed excitation emission in radioluminescence and cathodoluminescence at low temperatures.

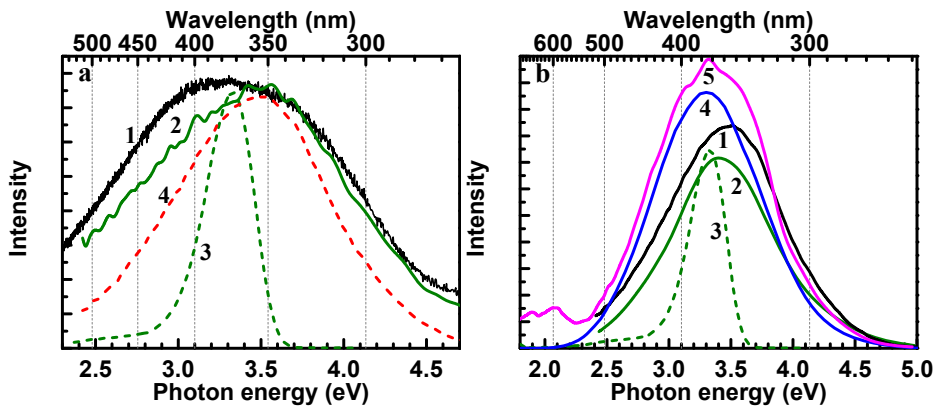


Fig. 11. a) Radioluminescence spectra of undoped $\text{Li}_2\text{B}_4\text{O}_7$ (1) and $\text{Li}_2\text{B}_4\text{O}_7:\text{Cu}$ (2) crystals at 4.2 K. For comparison, the photoluminescence of Cu^+ at the excitation energy 5.3 eV (3) and the STE emission at excitation energy 8.0 eV (4) are also presented for $\text{Li}_2\text{B}_4\text{O}_7:\text{Cu}$. **b)** Cathodoluminescence spectra of undoped $\text{Li}_2\text{B}_4\text{O}_7$ (1), $\text{Li}_2\text{B}_4\text{O}_7:\text{Cu}$ (2), $\text{Li}_2\text{B}_4\text{O}_7:\text{Ag}$ (4), and $\text{Li}_2\text{B}_4\text{O}_7:\text{Mn}$ (5) crystals at 5.3 K. For comparison photoluminescence of Cu^+ at $E_{\text{exc}}=5.3$ eV is presented for $\text{Li}_2\text{B}_4\text{O}_7:\text{Cu}$ (3).

4.3. Low-temperature TSL curves and lattice dynamics

Thermally stimulated luminescence was investigated in crystalline and ceramic samples irradiated either at low or room temperatures. Both TSL curves and spectra were studied in detail. In order to identify the centres responsible for TSL in various doped samples, the TSL spectra of irradiated samples were

compared with those measured from the same sample at the same temperatures under photostimulation.

The TSL curves of doped LTB single crystal and ceramic samples recorded in the range of 5–250 K after irradiation by an electron beam (5 kV, 0.3 μ A) at 5 K are shown in Figs. 12a and 12b. All samples clearly demonstrate a dominant TSL glow peak in the range of 60–120 K. In the case of LTB:Mn and LTB:Cu,Ag crystals, a substantially weaker peak can be traced in the region 140–170 K (Fig. 12. a, curve 3). Similar low temperature TSL curves have been earlier reported for LTB:Mn single crystals [56, 57]. The absence of weak background TSL peaks in the region of 150–300 K indicates that the grown doped single crystals are of good quality. The situation is somewhat different in the case of doped ceramics, where the presence of an additional glow peak is observed in the region of 190–230 K (Fig. 12b). The appearance of this peak depends strongly on sample preparation conditions and is related to some unidentified intrinsic or extrinsic defects.

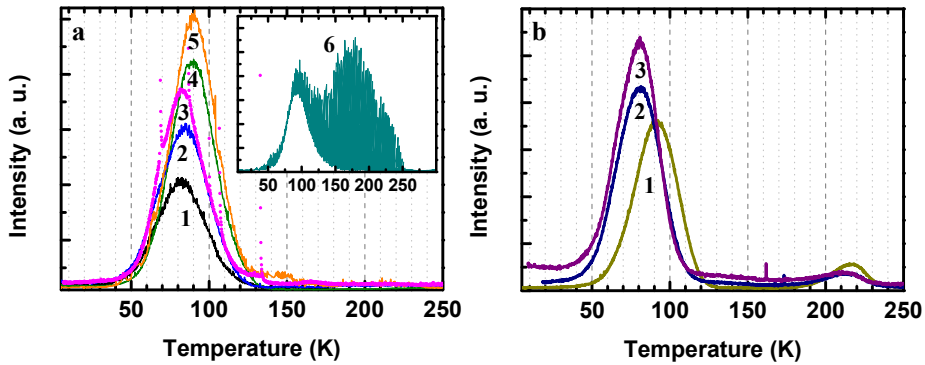


Fig. 12. a) Low-temperature TSL glow curves recorded from undoped and doped $\text{Li}_2\text{B}_4\text{O}_7$ single crystals irradiated by an electron beam at 5 K: $\text{Li}_2\text{B}_4\text{O}_7$ (1), $\text{Li}_2\text{B}_4\text{O}_7\text{:Ag}$ (2), $\text{Li}_2\text{B}_4\text{O}_7\text{:Mn}$ (3), $\text{Li}_2\text{B}_4\text{O}_7\text{:Cu}$ (4), $\text{Li}_2\text{B}_4\text{O}_7\text{:Cu,Ag}$ (5). The inset (6) depicts a glow curve recorded from a $\text{Li}_2\text{B}_4\text{O}_7\text{:Cu}$ crystal without a platinum coating on the crystal surface. **b)** The glow curves recorded from differently synthesised $\text{Li}_2\text{B}_4\text{O}_7\text{:Mn}$ ceramic samples after irradiation by an electron beam at 5 K: $\text{Li}_2\text{B}_4\text{O}_7\text{:Mn}$ (1, MnCO_3), $\text{Li}_2\text{B}_4\text{O}_7\text{:Mn}$ (2, KMnO_4 (0.25 mol%) – aggregates), $\text{Li}_2\text{B}_4\text{O}_7\text{:Mn}$ (3, KMnO_4 (0.25 mol%) – point defects).

The peak parameters for all the samples in the low temperature range either derived by using algorithm published in [95] or calculated by using the TLD-MC program [96] are shown in Table 4. It is important to note that the results are similar, independent of the method used to obtain the parameters. The analysis of the shape of the TSL curves for doped crystal and ceramic samples in the low temperature range shows that the main peak lies essentially in the same region of 76–90 K for all samples, demonstrating the first order kinetics

with activation energies 0.029–0.044 eV. This fact indicates that the recombination process is of a similar character in pure and doped samples, varying only slightly with dopant. The frequency factor values ($0.63\text{--}2.99\text{ s}^{-1}$) are also very close in all the samples studied. These extremely low values of frequency factor can be indicative of unusual recombination process taking place between trapped charge carriers in close pairs. Up to our works, it has been only shown by EPR studies that self-trapped holes or holes trapped near Li^+ vacancies disappear in this temperature region [97].

The inset in Fig. 12a presents a glow curve measured from a Cu doped sample without platinum coating, which demonstrates very strong pyroelectric effects in the range of 70–250 K that practically masks the 90 K glow peak. Similar observations have been done previously [39], and flashes of thermally stimulated luminescence have been reported in [44]. In order to avoid such effects, the 5 nm platinum coating was routinely applied on the surface of the crystalline samples used in our experiments, which either reduces or eliminates the pyroelectric flashes completely. These pyroelectric flashes distort the shape of the low-temperature TSL glow peak which may lead to appearance of false sub-peaks within the main peak. It is vital to note that these types of effects are substantially weaker in the case of ceramic samples.

Table 4. Parameters of the low-temperature peak calculated for undoped and doped LTB crystals and ceramics, maximum temperature (T_m), activation energy (E), and frequency factor (s).

Samples	$T_m(\text{K})$	$E(\text{eV})$	$s(\text{s}^{-1})$
$\text{Li}_2\text{B}_4\text{O}_7$	82	0.029	0.70
$\text{Li}_2\text{B}_4\text{O}_7:\text{Cu}$	87	0.039	0.98
$\text{Li}_2\text{B}_4\text{O}_7:\text{Ag}$	85	0.031	0.66
$\text{Li}_2\text{B}_4\text{O}_7:\text{Cu, Ag}$	90	0.039	2.99
$\text{Li}_2\text{B}_4\text{O}_7:\text{Mn}$	81	0.030	0.63
$\text{Li}_2\text{B}_4\text{O}_7:\text{Mn}$ (MnCO_3 prec.)	90	0.044	2.8
$\text{Li}_2\text{B}_4\text{O}_7:\text{Mn}$ (KMnO_4 prec., clustered)	78	0.031	1.05
$\text{Li}_2\text{B}_4\text{O}_7:\text{Mn}$ (KMnO_4 prec., point)	76	0.033	1.45

As indicated already in Section 4.2, the TSL spectra measured in crystals irradiated by X-rays or electrons were also rather similar apart from higher intensity and less noise in the case of electron irradiation. For that reason, the low-temperature TSL spectra will be shown only for electron-beam irradiated crystals. For reliable comparison with TSL emission spectra, the photoemission spectra of Cu^+ , Ag^+ , Mn^{2+} centres were measured at the temperatures corresponding to the maxima of the studied TSL peaks.

The TSL spectrum of an undoped crystals measured in the region 70–110 K contains a weak and broad band centered at 3.35 eV (370 nm) (Fig. 13, inset), which closely correspond to low temperature XRL and CL spectra shown in Fig. 11a and b. The TSL spectrum in the low-temperature peak of $\text{Li}_2\text{B}_4\text{O}_7\text{:Cu}$ crystal is also represented by one less broad band peaking at 3.4 eV (365 nm). Although its position is close to that of the Cu^+ emission recorded under photoexcitation, the TSL band at low temperatures is broader and certainly cannot be ascribed only to the electron transition within the Cu^+ ion (Fig. 13a). It might be composed of both Cu^+ emission and an emission originating from electron-hole recombination at an impurity-perturbed lattice site. The position of the TSL band is in good agreement also with that of radio- and cathodoluminescence measured for $\text{Li}_2\text{B}_4\text{O}_7\text{:Cu}$ crystals at low temperatures.

Contrary to the previous cases, the TSL spectrum measured within the interval of 70–100 K for LTB:Ag crystals does not correspond fully to the low-temperature cathodoluminescence spectrum. It is clearly seen from Fig. 13b that although the emission of Ag^+ ion is dominant, a wide band peaking around 3 eV (413 nm) is also present. The latter does not correspond to the self-trapped exciton emission. This band could be related to recombination of charge carriers at oxygen sites perturbed by an Ag^+ ion.

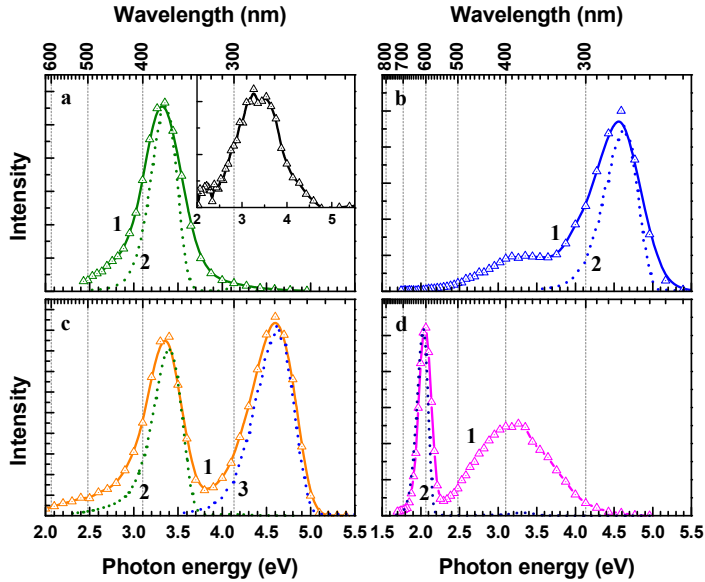


Fig. 13. TSL spectra of undoped $\text{Li}_2\text{B}_4\text{O}_7$ (inset), $\text{Li}_2\text{B}_4\text{O}_7\text{:Cu}$ (a, 1), $\text{Li}_2\text{B}_4\text{O}_7\text{:Ag}$ (b, 1), $\text{Li}_2\text{B}_4\text{O}_7\text{:Cu,Ag}$ (c, 1), $\text{Li}_2\text{B}_4\text{O}_7\text{:Mn}$ (d, 1) recorded in the ranges 76–81 K (inset), 83–88 K (a, 1), 80–86 K (b, 1), 90–95 K (c, 1), 75–80 K (d, 1) following the irradiation by an electron beam at 5 K as well as the photoemission spectra of $\text{Li}_2\text{B}_4\text{O}_7\text{:Cu}$ at $E_{\text{exc}}=5.3$ eV (a, 2 and c, 2), $\text{Li}_2\text{B}_4\text{O}_7\text{:Ag}$ at $E_{\text{exc}}=6.05$ eV (b, 2 and c, 3) and $\text{Li}_2\text{B}_4\text{O}_7\text{:Mn}$ at $E_{\text{exc}}=7.0$ eV (d, 2) recorded at the temperatures corresponding to the maxima of the studied TSL peaks.

The TSL spectra of $\text{Li}_2\text{B}_4\text{O}_7\text{:Cu,Ag}$ contain the fingerprints of both Cu^+ and Ag^+ ions. The spectrum of the 90 K peak contains the 3.35 eV (370 nm) emission, which can be clearly related to defect-related luminescence with an admixture of Cu^+ emission, and the emission of Ag^+ centres (Fig. 13c, curves 1, 2 and 3). It is important to indicate that also the phosphorescence spectra measured after irradiation by an electron beam at 5 K are composed of the emission originating from both Cu^+ and Ag^+ centres, indicating that tunnelling recombination takes place within close pairs of copper and/or silver ions of various valence states.

The TSL spectrum typical of $\text{Li}_2\text{B}_4\text{O}_7\text{:Mn}$ ceramics and single crystal samples recorded for the low-temperature peak situated in the range 75–80 K is shown in Fig. 13d. The spectrum for this peak was recorded for the first time. It is represented by two bands, a narrow one at 2.06 eV (600 nm) clearly related to Mn^{2+} ions and a broad one peaking at 3.26 eV (380 nm) attributed to oxygen-centred excitons disturbed by some intrinsic or extrinsic defect, e.g., a Mn^{2+} ion. The latter emission band is very similar to those observed in low-temperature TSL of undoped LTB and LTB doped with other impurities and resembles also room-temperature radioluminescence spectra reported earlier for LTB:Mn [56, 59]. The band around 380 nm (3.26 eV) is completely absent in high-temperature TSL. It is important to mention that in case of ceramic samples the relative intensities of these two bands differ slightly depending on manganese concentration in the bulk and synthesis method. Due to the reason of higher intensity at low temperatures only the spectrum recorded from LTB:Mn single crystal is presented on Fig. 13d.

As the low-temperature peaks in the region of 76–90 K (Fig. 12) are observed in undoped $\text{Li}_2\text{B}_4\text{O}_7$ and $\text{Li}_2\text{B}_4\text{O}_7$ doped with different impurities, it may be assumed that at least one of the recombination partners for these peaks is of intrinsic origin. It has been shown by the EPR method that hole-trapping centres are thermally destabilised at 90 K in LTB [97, 98]. Due to low crystal symmetry it was difficult to conclude whether the hole is self-trapped or stabilized by a Li^+ vacancy. The released holes can recombine with electrons localized at various traps, whereas the variety of trapping centres is expected to be wider in doped samples, giving rise to TSL with a higher intensity with respect to that in undoped samples.

The suggestion about the same nature of the processes involved is supported by the similarity of the TSL peak parameters in all crystals and ceramic samples presented in Table 4. In order to explain the exceptionally low value of the frequency factor, one has to refer to other abnormalities observed in lithium tetraborate in this temperature range. LTB crystals are known to behave unusually between 70 and 240 K according to a number of peculiarities reported by various authors. These provide us with additional information necessary to explain the recombination mechanisms responsible for the TSL processes at low temperatures. Very characteristic anomalies in thermal expansion and temperature dependences of the intensity of the Bragg reflection around 95 K have been reported in [99–102]. These were followed by a series of peculiarities in the region 100–240 K. Heat capacity anomalies [103] and a large decrease in

the off-axis pyroelectric coefficient at 80, 130, and 240 K have been found in [104]. Anomalies in elastic stiffness for the polar [001] direction were observed in the same temperature range at 75, 125, and 240 K, whereas the elastic stiffness minimum was observed around 75 K [105]. Finally, remarkable changes in the infra-red absorption spectra have been found at low temperatures. In the infra-red absorption spectra of LTB, two groups of bands at 800–1100 cm^{-1} and 1100–1400 cm^{-1} have been assigned to tetrahedrally and trigonally coordinated boron, respectively, while the peak at 420 cm^{-1} has been attributed to lithium [106]. Large-scale studies carried out on various lithium containing compounds allowed to assign the peaks in the region 300–510 cm^{-1} to Li^+ coordinated by four nearest oxygen neighbours [107]. The assignment has been confirmed in [108, 109], whereas it has also been shown that these bands are rather broad below 100 K and narrow at higher temperatures [108]. The low-temperature broadening has been attributed to the freezing of Li^+ ions in off-site positions below 100 K. A dynamic lithium disorder has been suggested for lithium tetraborate in the temperature range 100–200 K [42].

Considering the above-described anomalies, one can deduce the following model of the low temperature TSL processes in $\text{Li}_2\text{B}_4\text{O}_7$. At temperatures below 90 K, Li^+ ions occupy static irregular off-site positions, thus giving rise to a number of cation vacancies with uncompensated effective negative charge. The latter facilitate an efficient hole trapping at neighbouring oxygen ions. At temperatures around 90 K Li^+ ions become mobile and partially occupy native cation vacancies leading to the release of the associated oxygen holes. The holes recombine with electrons trapped at the nearest neighbouring oxygen vacancies or with impurity centres Cu^0 , Ag^0 , and Mn^+ [97] giving rise to the TSL peaks observed at these temperatures. Hole release in this case is an ionic process which does not correspond to a typical thermal activation of a hole, and for that reason one obtains unusually low frequency factor values (0.63–2.99 s^{-1}) when the standard glow curve treatment is applied in the TSL analysis. The spectral analysis of the low-temperature peaks shows that the recombination of mobile holes with trapped electrons takes place either on oxygen sites and the emission of excitons perturbed by Cu^+ , Ag^+ , or Mn^{2+} ions is observed at 3.4 eV (365 nm), 3 eV (413 nm), and 3.3 eV (375 nm), respectively, or at the dopant Cu^0 , Ag^0 , and Mn^+ centres and the characteristic Cu^+ , Ag^+ , and Mn^{2+} emissions at 3.35 eV (370 nm), 4.6 eV (270 nm), and 2.03 eV (610 nm) are observed (Fig. 13a-d).

The region 140–170 corresponds to the minimum of the crystal unit cell volume in the process of lattice rearrangement during the heating [42, 43]. The TSL curves of uncoated crystals exhibit the strongest and most frequent flashes in temperature interval 70–170 K, which are unavoidably integrated in TSL peaks. The flashes are not of true TSL origin and for that reason weak TSL peaks observed at 140–170 K for LTB:Mn and LTB:Cu,Ag crystals are ascribed to the imperfections of surface Pt coating.

4.4. TSL spectra and dosimetric properties

4.4.1. $\text{Li}_2\text{B}_4\text{O}_7\text{:Cu}$

The high-temperature group is represented by two peaks with maxima at 357 and 457 K in LTB:Cu (Fig. 14). It has to be mentioned that the peaks in the range of 340–370 K are fast fading and accordingly, from the dosimetric point of view, have no practical value. For that reason, peak parameters were calculated only for the high temperature peak above 400 K. In the case of $\text{Li}_2\text{B}_4\text{O}_7\text{:Cu}$, it correspond well to the dosimetric peaks reported also in other papers [24, 47–49, 50, 55, 75, 110,]. The dosimetric peak for LTB:Cu is of first order kinetics, situated at 457 K and has an activation energy of 1.57 eV which is close to that reported by Tiwary et al. [46] and Martini et al. [25]. The presence of the shoulder at high-temperatures close to 495 K can be observed as well. The corresponding peak has been shown to be of second order kinetics, while its maximum position to shift towards low-temperatures with increasing dose [25]. In the high-temperature range, the TSL spectra peaking at 3.4 eV (365 nm) correspond well to that of Cu^+ photoluminescence measured at the same temperature, indicating that the dopant related emission is dominant in all peaks (Fig 14a, b, c). As no emission of perturbed excitons is observed in the high-temperature peaks of Cu doped crystal, one can conclude that the recombination takes place at impurity ions. The most probable mechanism is the recombination of mobile electrons released from oxygen vacancies or Cu^0 centres with holes represented by Cu^{2+} centres. These results are in good agreement with the results of earlier EPR studies [45, 77, 110]. In particular, two types of Cu^0 centres and two types of Cu^{2+} centres have been identified using the EPR method, whereas only one of the Cu^{2+} centres is active in the TSL process [110]. It has been shown that both Cu^0 centres and active Cu^{2+} centres disappear at crystal heating in the region of the dosimetric TSL peak, in good accordance to our TSL data. It has been also suggested that electrons released from oxygen vacancies may be responsible for the peak in the region 340–370 K, however, no EPR signal from such centre has been detected in LTB:Cu [110].

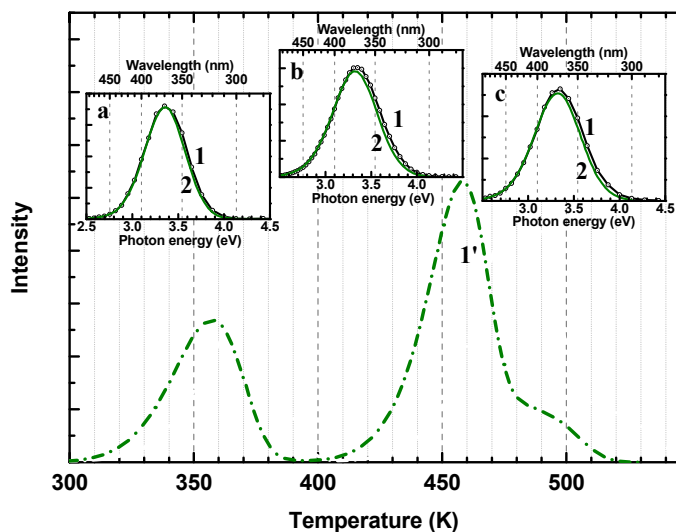


Fig. 14. TSL glow curves of a $\text{Li}_2\text{B}_4\text{O}_7\text{:Cu}$ single crystal irradiated by X-rays at 295 K (1'). The insets (a), (b), and (c) show TSL spectra of a $\text{Li}_2\text{B}_4\text{O}_7\text{:Cu}$ crystal in the range of 355–360 K (a, 1), 455–460 K (b, 1), and 490–500 (c, 1) compared with a photo-emission spectra of $\text{Li}_2\text{B}_4\text{O}_7\text{:Cu}$ recorded at 350 K (a, 2), 466 K (b, 2), and 500 K (c, 2) at excitation energy 5.3 eV.

4.4.2. $\text{Li}_2\text{B}_4\text{O}_7\text{:Ag}$

The TSL glow curve of LTB:Ag in high-temperature region is represented by two groups of peaks: a fast fading one in the region 320–370 K and a dosimetric one in the region 380–510 K (Fig 15). The latter is non-elementary indicating probably impurity aggregation processes in stored crystals. It is important to denote that the shape of the TSL curve and maximum position of the peak situated at 433 K, are exactly the same as reported earlier by Brant et al [54] for a heating rate 0.1 K/s. A “quick first estimation method” has been introduced by Randall and Wilkins for approximate determination of activation energy as $E=25kT_m$, where T_m corresponds to the peak temperature [111]. Depending on heating rate (0.1–0.5 K/s) the peak maximum has been shown to vary from 433 to 450 K and the activation energy from 0.93 to 0.97 eV. If such type of approximation method is used, a relatively high uncertainty exceeding 20% can be expected [54]. Recently Buchanan et al. [112] has shown by the comparison of EPR and TSL data, that the concentration of radiation induced centres related to Ag ions starts to decrease at 125 °C (398 K), resulting in appearance of TSL peak with maximum 170 °C (443 K).

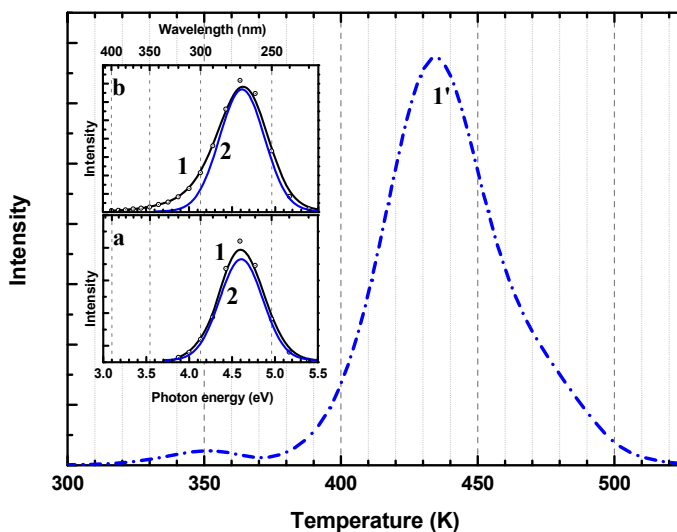


Fig. 15. TSL glow curve of a $\text{Li}_2\text{B}_4\text{O}_7\text{:Ag}$ single crystal irradiated by X-rays at 295 K (1'). The insets (a) and (b) show TSL spectra in the range of 345–350 K (a, 1) and 430–435 K (b, 1) compared with a photoemission spectra of $\text{Li}_2\text{B}_4\text{O}_7\text{:Ag}$ recorded at 350 K (a, 2) and 440 K (b, 2) at excitation energies 6.05 eV.

The study of high-temperature TSL spectra reveals that the 3 eV band, characteristic of low-temperature TSL, is absent in TSL peaks at 354 and 443 K and only the emission of the Ag^+ ion near 4.6 eV is present (Fig. 15, insets).

Similarly to the case of LTB:Cu , the luminescence spectroscopy data are in good accordance with the results of the EPR study of LTB:Ag crystals carried out earlier in [54, 112] and with the results of the spectroscopic study of Ag^{2+} centres in LTB:Ag [113]. Since only the 4.6 eV (270) emission is observed in the dosimetric peak of the LTB:Ag crystals, one can conclude that the recombination takes place at Ag impurity when mobile electrons from oxygen vacancies or Ag^0 centres recombine with holes localized at Ag^{2+} centres.

4.4.3. $\text{Li}_2\text{B}_4\text{O}_7\text{:Cu,Ag}$

The high temperature group of TSL peaks of LTB:Cu,Ag is represented by the bands situated at 344, 420 and 480 K. The position of the 480 K peak in LTB:Cu,Ag is close to the position of a high temperature shoulder in LTB:Cu . In LTB:Cu,Ag , an activation energy for the dosimetric peak at 420 K is 1.14 eV. Similar value of the activation energy 1.13 eV has been determined in an LTB sample triple-doped with Cu, Ag, and P for a heating rate of 1 K/s [50].

The TSL spectra of $\text{Li}_2\text{B}_4\text{O}_7\text{:Cu,Ag}$ display the emissions of Cu^+ and Ag^+ ions. While the TSL peaks at 344 K and 440 K are presented by the emission of both impurities, the peak at 480 K shows only the Cu^+ emission (Fig. 16). These data are in good agreement with those reported in [75].

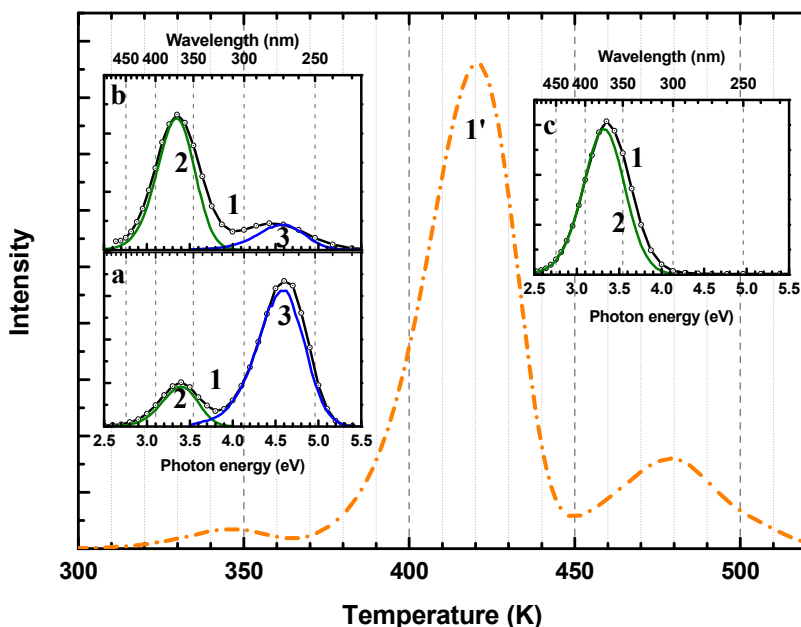


Fig. 16. TSL glow curve of $\text{Li}_2\text{B}_4\text{O}_7:\text{Cu,Ag}$ single crystal irradiated by X-rays at 295 K (1'). The insets (a), (b), and (c) show a TSL spectra of an $\text{Li}_2\text{B}_4\text{O}_7:\text{Cu,Ag}$ crystal in the range of 340–345 K (a, 1), 345–350 K (b, 1), and 488–493 K (c, 1) compared with a photoemission spectra of $\text{Li}_2\text{B}_4\text{O}_7:\text{Ag}$ and $\text{Li}_2\text{B}_4\text{O}_7:\text{Cu}$ recorded at 340 K (a, 2), 440 K (b, 2), and 480 K at excitation energies 6.05 eV and 5.3 eV, respectively.

Taking into account the previous EPR study results reported by [45, 54, 110, 112] and spectroscopic results presented in the current theses, it can be concluded that at high temperatures the recombination takes place exclusively on impurity ions. Most probably electrons are released from oxygen vacancies or $\text{Cu}^0(\text{Ag}^0)$ and recombine with hole centres represented by $\text{Cu}^{2+}(\text{Ag}^{2+})$ centres. If the suggestion of Brant et al. [110] that electron release from oxygen vacancies is responsible for the fast fading peak in the region of 340–370 K is correct, then it has to be admitted that co-doping with silver changes the surrounding environment of oxygen vacancies, because the 357 K peak observed in the $\text{LTB}:\text{Cu}$ is suppressed in a crystal co-doped with Ag and a new peak at 344 K appears in it.

4.4.4. $\text{Li}_2\text{B}_4\text{O}_7:\text{Mn}$ single crystal

The high-temperature group of TSL peaks and the TSL spectra measured at temperatures corresponding to the peak maxima are presented in Fig. 17. The TSL curves were measured for the same crystal sample sequentially irradiated by X-rays to four increasing doses: 1.2, 3.6, 7.2 and 14.4 kGy. After each TSL

curve measurement the sample was heated to 700 K, kept at that temperature for 10 minutes and cooled down to room temperature. It is clearly seen that while the position of the first peak remains in these measurements the same, the maximum of the dosimetric peak drifts from 510 K at the dose of 1.2 kGy to 470 K at 14.4 kGy. This shift is accompanied by the change of the peak shape from asymmetric to almost symmetric which is characteristic of second order kinetics involving re-trapping of charge carriers in the process of recombination (see, e.g., [114]). The dependence of the integral intensity of the dosimetric peak on irradiation dose is linear. The emission spectrum remains the same for both peaks of the high-temperature group for all irradiation doses and corresponds to the emission of Mn^{2+} centres under photoexcitation.

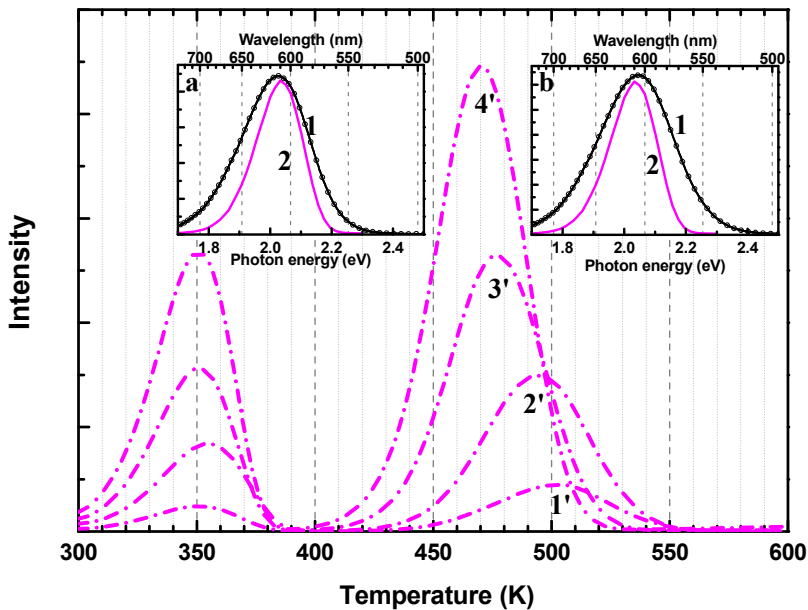


Fig. 17. TSL glow curve of a $\text{Li}_2\text{B}_4\text{O}_7:\text{Mn}$ crystal irradiated by X-rays with the dose of 1.2 (1'), 3.6 (2'), 7.2 (3'), and 14.4 kGy (4'). TSL spectra (1) measured in the region of 330–370 K (inset a) and 450–520 K (inset b) compared to the Mn^{2+} centre emission measured under photoexcitation at RT (2 in both insets).

The displacement of a TSL peak with irradiation dose is not typical. A similar effect has been observed in a similar dose interval in γ -ray irradiated LTB:Mn crystals [58], however, the shift was of opposite direction. A somewhat irregular displacement of the dosimetric peak with irradiation dose has been observed for γ -irradiated polycrystalline powders, though with a shift towards low temperatures for high irradiation doses [115]. The nature of the observed shift of the dosimetric peak is not yet clear, however, one can suggest a transformation of

the trapping and luminescence centres in the process of lattice rearrangements during repeated heating and cooling of the sample. The transformation may also be facilitated by crystal irradiation. The important role of ionic mobility in the processes of reversible Mn segregation in LTB:Mn has been recently described in Ref. [116]. A solid argument in favour of changing centre configuration was obtained by measuring low-temperature emission and excitation spectra of an LTB:Mn crystal which had undergone numerous irradiation and heating cycles (Fig. 18). Beside the red emission at 2.03 eV possessing a well resolved series of excitation bands in the visible-to-UV region, such samples demonstrated under UV excitation a more intense emission band at 2.36 eV (525 nm) with only a shoulder on the red side of the spectrum (curve 1). The excitation spectrum of this green emission was much less structured (curve 1'), though the regions of most intense excitation bands are similar to those of the 2.03 eV emission. It is remarkable, that the recombination luminescence of such sample is still dominated by the 2.03 eV band in TSL measurements. A similar disagreement between the emission spectra recorded under photoexcitation of unirradiated samples and during the thermal stimulation of irradiated samples has been found for LTB:Mn powders [115]. All these data indicate that a considerable amount of Mn^{2+} centres are capable of changing their coordination number in the course of repeated irradiation and heating of LTB:Mn samples, however, the centres active in the processes responsible for TSL remain mainly those yielding the red emission. It is worth to note that 2.03 eV is dominant in all studied samples under the VUV excitation in the region 6.5–8 eV.

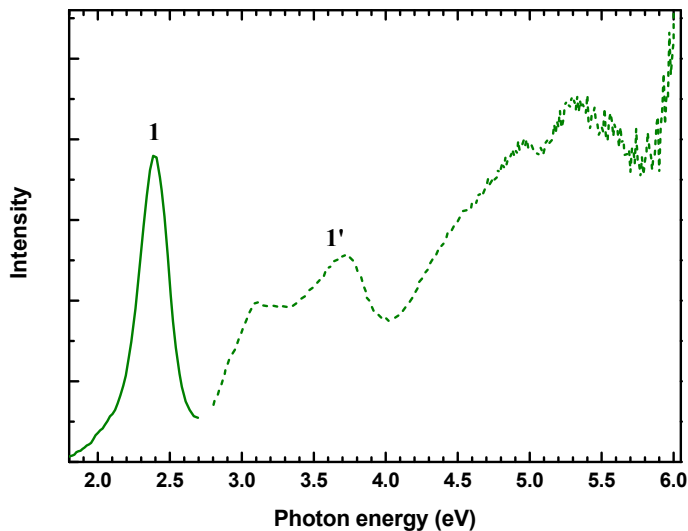


Fig. 18. Emission (1) and excitation (1') spectra measured at 4.2 K for an LTB:Mn crystal repeatedly irradiated at RT and heated to 700 K.

In our opinion, a stochastic process of lattice rearrangement around impurity ion or their pairs and clusters cannot fully explain the dose shift of the dosimetric TSL peak. One can suggest that the rearrangement is to some extent random and depends on material morphology (powder, crystal), impurity concentration and preparation method, causing different level of strain in the material during growth and cooling procedures. This can explain some irregularity of TSL peak displacements observed in Refs. [58, 59, 115]. A regular shift of the dosimetric TSL peak with dose in crystal is unlikely to be caused by the lattice rearrangement only. A model of the process can be suggested based on our Q-band EPR results finding only Mn^{2+} ions substituted for Li^+ ions in LTB:Mn crystals. In this case the concentration of other doping-related defects, except charge compensating lithium vacancies, should be rather low, this inevitably meaning that impurity recharging processes are most important in irradiated crystals, as already proposed by Ignatovich et al. [47]. In such a model, a hole created by ionizing radiation gets trapped as a Mn^{3+} ion, while another Mn^{2+} traps an electron with the formation of a Mn^+ ion. The relative number of other potential deep electron traps like oxygen vacancies is supposed to be small in manganese doped crystals due to the excess of positive charge in the lattice provided by Mn^{2+} ions substituted for Li^+ . The circumstance that both hole and electron traps are related to Mn impurities explains the linear dependence of TSL intensity on irradiation dose in wide range of doses [3]. In this picture, the recombination of trapped electrons and holes involves pairs of manganese ions, their mean distance decreasing for high irradiation doses, which can lead to a low temperature shift of the dosimetric peak [117]. The presence of two TSL peaks above RT can be explained by the mobility of Li vacancies (V_{Li}) in the following way. In as grown crystals, Mn^{2+} is always charge compensated by an adjacent V_{Li} . During the capturing of an electron with surplus energy part of the $\text{Mn}^+ - V_{\text{Li}}$ complexes may get dislocated due to a high mobility of Li^+ ions. The remaining $\text{Mn}^+ - V_{\text{Li}}$ complexes are less stable and will lose the surplus electron above RT producing the fast-fading TSL peak, while the Mn^+ ions left alone stay stable up to ~ 500 K and yield the dosimetric peak. This process may be influenced by the local Mn concentration, explaining the varying relative intensities of the two TSL peaks. The $\text{Mn}^{3+} - V_{\text{Li}}$ complexes formed by hole capture are either stable enough or may acquire another V_{Li} with increasing temperature. In all cases the recombination takes place at Mn^{3+} centres, resulting in the Mn^{2+} emission. The scenario described here for crystals is different from that suggested earlier for ceramic samples [63, 64] clearly requiring a careful verification of the latter in view of our EPR results on LTB:Mn crystals and ceramics. In particular, it would be important to find a method for detecting Mn^+ and Mn^{3+} ions in the material.

4.4.5. $\text{Li}_2\text{B}_4\text{O}_7\text{:Be}$, $\text{Li}_2\text{B}_4\text{O}_7\text{:Mn}$ and $\text{Li}_2\text{B}_4\text{O}_7\text{:Mn,Cu}$ ceramics

In order to help identify the sign of the recombination process taking place in the dosimetric peak in LTB:Mn ceramics, LTB:Be ceramics were synthesised. It has been proposed that Be^{2+} substitutes for both Li^+ and for B^{3+} in $\text{Li}_2\text{B}_4\text{O}_7$, resulting in appearance of an effective electron and hole trapping centres [63]. Beryllium is a prominent compound for EPR studies due to the recognizable hyperfine structure in EPR spectra (^9Be possesses a nuclear spin of $3/2$), which was supposed to help identifying the position of related trapped charge carries.

In Fig. 19, the EPR spectrum of $\text{Li}_2\text{B}_4\text{O}_7\text{:Be}$ recorded at 77 K is presented. The EPR measurements were performed after X-irradiation of the sample with a dose of 1.2 kGy. The spectrum is composed of four lines of the hyperfine structure, due to hyperfine interaction with ^9Be nuclei. The observed splitting is ($A=0.92 \pm 0.05$ mT) and corresponds to an unpaired electron located in the proximity of the ^9Be nucleus. The observed centre has an anisotropic g-factor with one component situated close to that of a free electron (not resolved in the spectrum), and two positively shifted components, which is a common feature for hole centres related to O^- in oxides. A hyperfine structure composed of four lines could be expected also in the case of hyperfine interaction with ^{11}B nuclei. However, the splitting caused by ^{11}B [97] is about twice as small ($0.46\text{--}0.58$ mT) as in the case of ^9Be . The positively charged Be^{2+} ion substituting for Li^+ cannot be responsible for the appearance of hole traps. One of the possibilities of hole trapping may appear when Be^{2+} substitutes for B^{3+} in tetrahedral BO_4 , resulting in hole capturing at an oxygen ion bridging between two BO_4 units where Be^{2+} substitutes at the tetrahedral B^{3+} site.

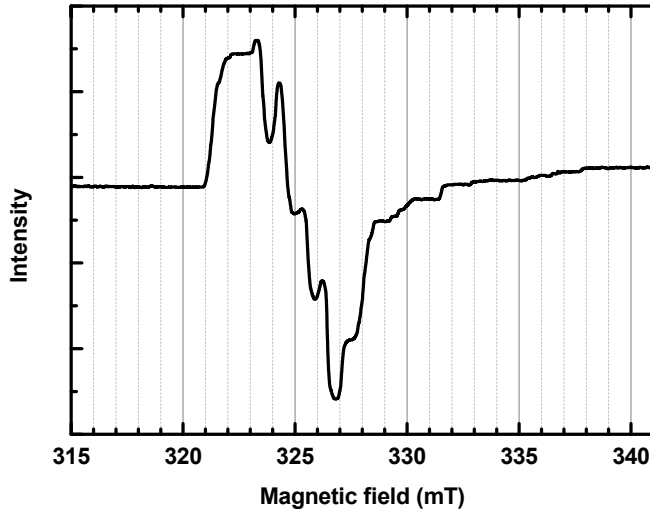


Fig. 19. EPR spectrum (X-band modulation at 975 kHz) of a radiation induced trapped-hole centre in $\text{Li}_2\text{B}_4\text{O}_7\text{:Be}$ recorded at 77 K after X-irradiation.

The same hole-capturing site has been proposed by Swinney for an undoped LTB single crystal [97], where the electrons are trapped at oxygen vacancies and holes are stabilized by lithium vacancies. The hole-centres in the case of the latter become unstable around 90 K. The hole localised near Be^{2+} substituting for B^{3+} exhibits a higher thermal stability. It is also important to note that in the case of $\text{Li}_2\text{B}_4\text{O}_7\text{:Be}$ the hyperfine structure g-tensor value for the trapped hole centre is ($g=2.0110 \pm 0.0005$) which is similar to that reported for the holes in undoped crystals [97].

The TSL glow curve recorded in the temperature interval 290–685 K after sample irradiation by a metrological class ^{239}Pu radiation source at room temperatures is shown for $\text{Li}_2\text{B}_4\text{O}_7\text{:Be}$ in Fig. 20, curve 1'. A fast fading peak in the region of 325–373 K, a dosimetric peak in the region of 510–575 K and a considerably weaker one at 450 K can be distinguished. The peak at 325–373 K clearly demonstrates the first kinetics order, having activation energy of 0.6 eV. Its TSL spectrum contains a narrow band centred near 2.1 eV and substantially wider one close to 3.5 eV (Fig. 20a). The former red luminescence near 2.1 eV can be related to a casual Mn impurity and the latter to the Cu^+ luminescence. The band at 4.6 eV is probably related to Ag^+ , all together indicating that material studied was not of sufficient purity.

Taking into account EPR and TSL results it may be suggested that the peak in the region of 325–373 K originates from a thermally activated recombination of a hole stored at the bridging oxygen (near Be^{2+} at tetrahedral B^{3+} position) with an electron trapped in close vicinity. The absence of re-trapping favours the model of recombination in close pairs.

The TSL spectrum recorded for the dosimetric peak maximum in the region of 510–575 K is dominated by band between 3 and 4 eV, while weaker luminescence bands belong to residual unintentional impurities, e.g. Mn^{2+} (Fig. 20b). The interaction of Mn and Be ions in LTB:Mn,Be has been discussed in more detail in [64]. The high-temperature peak in the region of 510–575 K correlates well with the annealing of the EPR signal of the hole-centre (Fig. 20, curve 2'). The result on a single-stage annealing of the paramagnetic centre are in a good agreement with the idea that released holes recombine with some trapped electrons, giving rise to high-temperature TSL peak. It can be supposed that the electron traps appear when Be^{2+} ions substitute for Li^+ sites. The states at the conduction band minimum are built of the antibonding BO_3 -orbitals. In the case of Be^{2+} substitution into Li^+ site, these orbitals are suggested to split from the conduction band resulting in creation of electron traps in the bandgap. Electron trapping on the antibonding BO_3 has been expected to be energetically more preferable compared to a charge transformation of Be^{2+} , as charge transformation would cause the increase of Be ion radius, causing additional distortions in the surrounding crystal structure [64]. Due to that, it is proposed that the high-temperature peak in the region of 510–575 K is observed when the holes trapped at bridging oxygen are thermally released and recombine with the electrons trapped at the antibonding BO_3 orbitals.

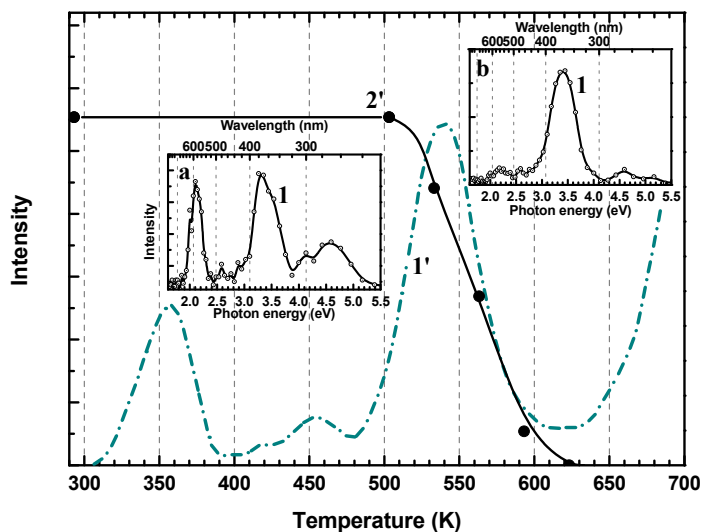


Fig. 20. TSL glow curve of a $\text{Li}_2\text{B}_4\text{O}_7\text{:Be(0.13 mol\%)}$ ceramic sample irradiated with a ^{239}Pu source for 100 s (1') and the annealing of EPR signal of the radiation-induced centre (2') recorded with a linear heating rate 0.15 K/s. Insets: TSL spectra for $\text{Li}_2\text{B}_4\text{O}_7\text{:Be(0.13 mol\%)}$ recorded in the range of 342–354 K (a,1) and 538–553 K (b,1).

The glow curve of $\text{LTB:Mn (0.13 mol\%)}$ irradiated during 100 s at RT with a ^{239}Pu radiation source is shown in Fig. 21, curve 1'. It contains two main TSL peaks in the regions of 335–345 and 470–510 K. The former is subject to fast fading at RT and has no practical importance. The high-temperature peak is very stable and for that reason is perspective from the viewpoint of thermal readout of the stored radiation dose. The processes responsible for the recombination luminescence in these peaks are suggested to be the same as described for LTB:Mn crystals in the previous section. The emission spectrum of the TSL measured in the maximum of the dosimetric peak is close to the photoluminescence spectrum measured at RT (Fig. 21a). Correspondingly, the recombination takes place at the Mn^{2+} ion.

Finally, we found that the dosimetric peak is observed practically at the same temperatures in $\text{Li}_2\text{B}_4\text{O}_7\text{:Mn}$ ceramics co-doped with Cu^+ (Fig. 21, curve 2'), which has been shown to substitute exclusively for Li^+ ions, but to occupy slightly off-site position [45, 110]. In this case, the Cu^+ ion emission peaked at 3.35 eV can be observed in result of the recombination of an electron released from Mn^+ ion with an active Cu^{2+} centre (see section 4.4.1). It was found that under the same irradiation conditions the integral TSL intensity in $\text{Li}_2\text{B}_4\text{O}_7\text{:Mn,Cu}$, even with non-optimized impurity concentrations, is higher than that in $\text{Li}_2\text{B}_4\text{O}_7\text{:Mn}$, which provides an essential tool for increasing the sensitivity the material to ionizing radiation. Further studies on LTB:Mn ceramics co-doped with metal impurities in order to increase the number of relevant charge carrier traps are planned.

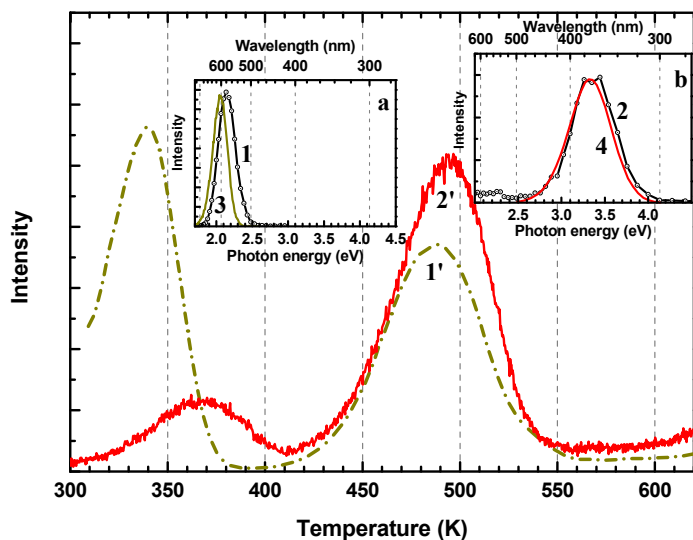


Fig. 21. TSL glow curves of the $\text{Li}_2\text{B}_4\text{O}_7\text{:Mn}(0.13 \text{ mol}\%)$ and $\text{Li}_2\text{B}_4\text{O}_7\text{:Mn}(0.13 \text{ mol}\%), \text{Cu}(0.13 \text{ mol}\%)$ ceramics irradiated with a ^{239}Pu radiation source for 100 s (1') or X-ray tube (20 kV, 0.4 mA) for 20 min at 295 K (2'), respectively. Insets: a TSL spectrum of $\text{Li}_2\text{B}_4\text{O}_7\text{:Mn}(0.13 \text{ mol}\%)$ and $\text{Li}_2\text{B}_4\text{O}_7\text{:Mn}(0.13 \text{ mol}\%), \text{Cu}(0.13 \text{ mol}\%)$ recorded in the range of 498–515 K (a,1) and 475–500 K (b,2), compared to the PL spectra of Mn^{2+} (a,3) and Cu^+ (b,4) centres recorded at 300 K and 490 K for $\text{Li}_2\text{B}_4\text{O}_7\text{:Mn}(0.13 \text{ mol}\%)$ and $\text{Li}_2\text{B}_4\text{O}_7\text{:Mn}(0.13 \text{ mol}\%), \text{Cu}(0.13 \text{ mol}\%)$, respectively.

By analysing the EPR signal in unirradiated LTB:Mn ceramics exhibiting partly resolved hyperfine splitting of the order of several mT it has been proposed by [63] that Mn^{2+} ions are capable of occupying two different sites in LTB lattice, either substituting for a Li^+ ion or breaking the boron-oxide network and substituting for B^{3+} in a fourfold-coordinated site. These proposals are inconsistent with the EPR studies carried out in the Q-band (microwave frequency $f = 33.818 \text{ GHz}$) revealing manganese dominantly incorporated in the crystal lattice as Mn^{2+} ions substituting for Li^+ ions. Although the ceramics samples were not studied in detail by the Q-band EPR, the comparison of the spectra measured for the disintegrated crystals and ceramics in the X-band showed that the Mn^{2+} ions are of the same type in both materials. Correspondingly, Mn^{2+} ions occupy Li^+ sites in ceramics and impurity recharging is important for the TSL processes in ceramics as well. In this connection, the mechanisms of energy storage and recombination luminescence of ceramics have to be re-examined taking advantage of the circumstance that impurity concentration and its distribution in the lattice can be controlled by ceramic preparation methods as shown below. In turn, the studies of the EPR spectra of defect-related electron and hole trapping centres, accompanying the main Mn^+ and Mn^{3+} centres in irradiated crystals, and their behaviour in temperature induced recombination processes can help revealing the nature (hole or electron) of the recombination reaction.

The EPR spectrum of one of such centres recorded at RT after X-irradiation of $\text{Li}_2\text{B}_4\text{O}_7\text{:Mn}$ is shown in Fig. 22, inset (for demonstration purposes a high dose about 11 kGy was used). In addition to the Mn^{2+} lines seen in non-irradiated samples [63] a new sextet structure with a splitting of the order of 1 mT can be discerned in the region 325–330 mT. This may correspond to a radiation centre with the unpaired spin having super-hyperfine interaction with a neighbouring Mn nucleus. The recorded spectrum only corresponds to one of the principal values of the g-tensor ($g=1.997 \pm 0.001$). The nature of this centres is not yet clear, as its g factor shift corresponds to electron, while the splitting is similar to that of a hole centre localized near a Be^{2+} ion in LTB:Be.

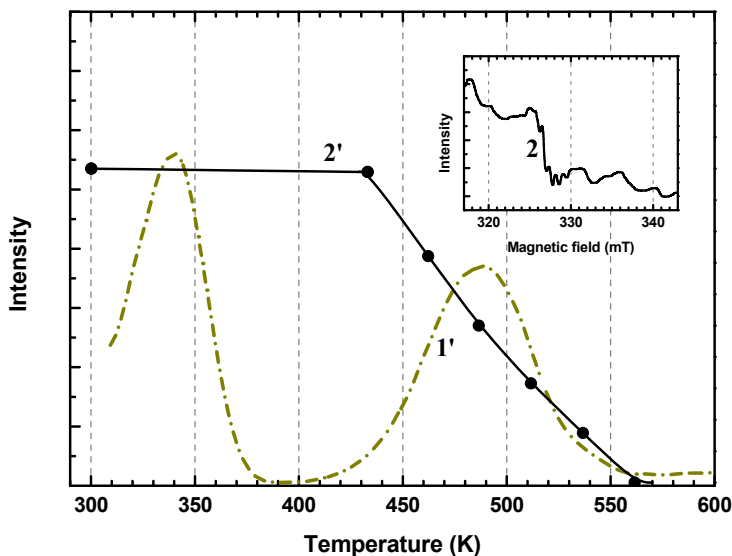


Fig. 22. TSL glow curve of a $\text{Li}_2\text{B}_4\text{O}_7\text{:Mn}$ (0.13 mol%) ceramic sample irradiated with a ^{239}Pu source for 100 s (1') and the annealing of EPR signal of the radiation-induced centre (2') recorded with a linear heating rate 0.15 K/s. Inset: an EPR spectrum of a radiation-induced centre recorded at RT after X-ray irradiation (2).

Whatever the nature of the centre under discussion, its EPR signal completely disappears exactly in the temperature region of the dosimetric peak at 490 K (Fig. 22, curve 2). Consequently, this centre is one of the partners in the recombination luminescence process responsible for the dosimetric peak. To reveal the sign of the observed process, one needs to co-dope LTB ceramics with impurities, which are capable of predominant trapping holes or electrons, and to follow their behaviour in dosimetric process. Our preliminary experiments with $\text{Li}_2\text{B}_4\text{O}_7\text{:Mn,Be}$ samples did not give reliable results because of strong overlapping of dosimetric peaks in LTB:Be and LTB:Mn.

4.4.6. Controlling dosimetric performance of ceramics by preparation methods

In order to control the properties of ceramic samples dependent on preparation and doping methods, the LTB:Mn ceramics containing manganese in clustered and uniformly distributed form, labelled as LTB:Mn(aggregate) and LTB:Mn(point defects), respectively, were prepared using the two different methods of doping, described in section 3.1.2.

The high-temperature TSL study after irradiation by an X-ray tube (W anode, 50 kV, 15 mA) for 2 min at RT was carried out on both types of the developed samples. The TSL curve of the LTB:Mn(point defects) sample contained two main peaks with maxima at 335 and 511 K, whereas in the case of LTB:Mn(aggregate), the peaks were shifted towards high temperatures resulting in maxima at 342 and 517 K (Fig. 23, curves 1' and 2', respectively). The main dosimetric peak at 511 K recorded for the LTB:Mn(point defects) sample is more symmetric, and resembles that recorded for the LTB:Mn single crystals at low irradiation doses (Fig. 17). In the case of the LTB:Mn(aggregate) sample, the dosimetric peak in the region of 420–600 K exhibits a more complex shape (see also [118]), differing by an additional shoulder close to 550 K. Nevertheless, the TSL spectra recorded for both irradiated samples revealed only the presence of the manganese related emission close to 2.1 eV in the whole high-temperature region studied (Fig. 23, inset).

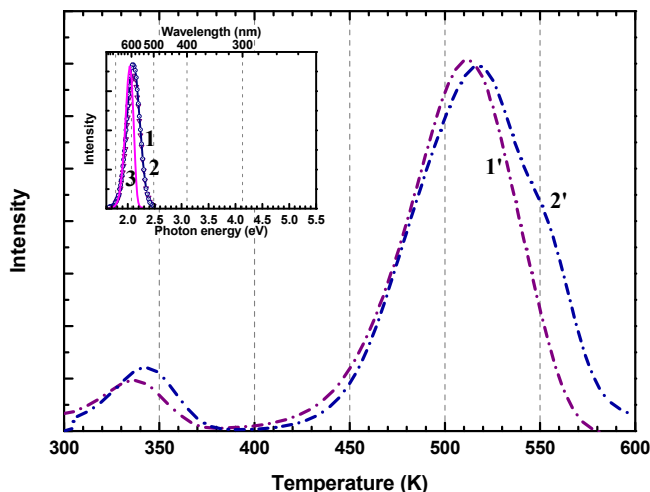


Fig. 23. TSL glow curves of $\text{Li}_2\text{B}_4\text{O}_7\text{:Mn}(\text{KMnO}_4, 0.25\text{mol}\%, \text{point defects})$ (1') and $\text{Li}_2\text{B}_4\text{O}_7\text{:Mn}(\text{KMnO}_4, 0.25 \text{ mol}\%, \text{aggregates})$ (2') ceramics irradiated with a X-ray tube (50 kV, 15 mA) for 2 min at 295 K. Inset: TSL spectra of the $\text{Li}_2\text{B}_4\text{O}_7\text{:Mn}(\text{KMnO}_4, 0.25\text{mol}\%, \text{point defects})$ (1) and $\text{Li}_2\text{B}_4\text{O}_7\text{:Mn}(\text{KMnO}_4, 0.25 \text{ mol}\%, \text{aggregates})$ (2) recorded in the range of 509–519 K (1) and 502–512 K (2), compared with to the PL spectrum of Mn^{2+} (3) centres recorded at 300 K for $\text{Li}_2\text{B}_4\text{O}_7\text{:Mn}(\text{KMnO}_4, 0.25\text{mol}\%)$.

The most remarkable result is that the TSL intensity of the main dosimetric peak under the same irradiations conditions in the LTB:Mn(point defects) sample is by factor of three higher than in the case of LTB:Mn(aggregate) sample, indicating a substantially higher sensitivity to ionizing radiation.

Although the full optimisation of impurity concentration and preparation conditions has not been performed and further studies of dose response linearity are needed, it can be already concluded that careful choice of synthesis methods and conditions can lead to improved control over the properties of the LTB:Mn dosimetric material.

SUMMARY

In the present work, thermostimulated luminescence of undoped lithium tetraborate ($\text{Li}_2\text{B}_4\text{O}_7$, or LTB), $\text{Li}_2\text{B}_4\text{O}_7\text{:Cu}$, $\text{Li}_2\text{B}_4\text{O}_7\text{:Ag}$, $\text{Li}_2\text{B}_4\text{O}_7\text{:Cu,Ag}$ and $\text{Li}_2\text{B}_4\text{O}_7\text{:Mn}$ crystals as well as $\text{Li}_2\text{B}_4\text{O}_7\text{:Mn}(\text{MnCO}_3)$, $\text{Li}_2\text{B}_4\text{O}_7\text{:Mn}(\text{KMnO}_4)$, $\text{Li}_2\text{B}_4\text{O}_7\text{:Mn,Be}$, and $\text{Li}_2\text{B}_4\text{O}_7\text{:Be}$ ceramics suitable for tissue equivalent dosimetry were investigated by the luminescence and EPR spectroscopy methods in a wide temperature range of 4.2–700 K. The main purpose of the study was to reveal the mechanisms of energy transfer, charge carrier storage and recombination relevant for dosimetric application of the materials studied.

The following results were obtained:

- The origin of the impurity luminescence of LTB:Ag and LTB:Cu,Ag crystals was clarified. It was shown that in the case of LTB:Ag the emission band with the maximum near 4.6 eV is due to the $5s \rightarrow 4d$ transition of Ag^+ ion. Theoretical calculations showed that the excitation bands in the region of 6.05 eV and 7.0–7.7 eV are related to the $4d \rightarrow 5s$ and $4d \rightarrow 5p$ transitions, respectively. It was shown that in the case of LTB:Cu,Ag crystal the emission of Ag^+ centres at 4.62 eV overlaps with the lowest-energy component of the Cu^+ centres absorption band at 4.7 eV. This fact indicates that Ag^+ can play a sensitizer role for Cu^+ emission. Energy transfer from Ag^+ to Cu^+ in LTB:Cu,Ag crystals is clearly demonstrated by the presence of the Ag^+ related shoulder at 6.1 eV in the excitation spectrum of Cu^+ emission.
- In the case of LTB:Mn crystal, two kinds of Mn^{2+} related emission bands were found in studied crystals. One peaking at 2.03 eV is detected in as-grown crystal under photoexcitation and in the thermostimulated luminescence of irradiated crystals. Another emission peaking in the region of 2.25–2.36 eV is observed in the crystals which have undergone numerous repeated irradiation and heating cycles. In the case of as-grown crystals, the observed excitation bands in the UV-Vis region, recorded for the 2.03 eV emission, were assigned to various transitions within the $3d^5$ electronic configuration of Mn^{2+} ions on the basis of the Tanabe-Sugano diagram. It was suggested that the doublet in the excitation spectra in the region of 7–8 eV corresponds to spin-allowed electronic transitions and is most likely related to the $3d^5 \rightarrow 3d^4 4s$ transitions of a Mn^{2+} ion populating the ^6D term split by crystal field in two subbands. It is important to note that these bands have not been reported before for LTB:Mn single crystal.
- The EPR studies performed for LTB:Mn for the first time in the Q-band (microwave frequency $f = 33.818$ GHz) showed that manganese is dominantly incorporated in the crystal lattice as Mn^{2+} ions substituting Li^+ ions. Based on these data, a model of the recombination luminescence relevant to the dosimetric peak, involving the impurity recharging processes and lattice rearrangement, is suggested.
- It was shown that the radioluminescence and cathodoluminescence spectra of pure and doped LTB crystals at low temperatures are dominated by

exciton-like emission caused by the recombination of charge carriers at regular oxygen lattice sites or at the oxygen lattice sites, which are perturbed by a lattice defects or an impurity ion.

- For the first time it is shown that TSL processes are strongly influenced by lattice rearrangements in LTB. According to the model suggested, at temperatures below 90 K, Li^+ ions occupy static irregular off-site positions, giving rise to a number of cation vacancies with uncompensated effective negative charge, leading to an efficient hole trapping at neighbouring oxygen ions. At temperatures close to 90 K Li^+ ions become mobile and partially occupy native cation vacancies leading to the release of the associated oxygen holes, followed by their recombination with electrons trapped at the neighbouring oxygen vacancies or various impurity centres giving rise to the TSL peaks observed in the region of 76–90 K. This process related to ionic mobility does not correspond to a typical thermal activation of a hole, and due to that unusually low frequency factor values are obtained when the standard glow curve treatment is applied.
- It was shown that the dosimetric peak at 490 K is observed practically at the same temperatures in LTB:Mn ceramics and in the samples co-doped with Cu^+ . Under the same irradiation conditions the integral TSL intensity of LTB:Mn,Cu is higher than that in LTB:Mn, thus demonstrating an increased sensitivity of the co-doped material to ionizing radiation.

SUMMARY IN ESTONIAN

Rekombinatsioonluminestsents lisanditega boraatides: tekkepõhjus ja rakendusperspektiivid dosimeetrias

Käesoleva töö raames uuriti kudeekvivalentse dosimeetria rakendusteks perspektiivseid materjale, lisandamata ning vase, hõbeda ja mangaaniga lisandatud liitiumtetraboraadi (LTB) ($\text{Li}_2\text{B}_4\text{O}_7$, $\text{Li}_2\text{B}_4\text{O}_7\text{:Cu}$, $\text{Li}_2\text{B}_4\text{O}_7\text{:Ag}$, $\text{Li}_2\text{B}_4\text{O}_7\text{:Cu,Ag}$ ja $\text{Li}_2\text{B}_4\text{O}_7\text{:Mn}$) monokristalle ning mangaani, vase ja berülliumiga lisandatud $\text{Li}_2\text{B}_4\text{O}_7\text{:Mn}(\text{MnCO}_3)$, $\text{Li}_2\text{B}_4\text{O}_7\text{:Mn}(\text{KMnO}_4)$, $\text{Li}_2\text{B}_4\text{O}_7\text{:Mn,Cu}$, $\text{Li}_2\text{B}_4\text{O}_7\text{:Mn,Be}$, $\text{Li}_2\text{B}_4\text{O}_7\text{:Be}$) keraamikaid termostimuleeritud luminestsentsi ja EPR meetoditel laias temperatuuride vahemikus 4.2–700 K. Töö põhieesmärgiks oli selgitada dosimeetrilisteks rakendusteks tähtsaid laengukandjate rekombinatsiooni protsesse, tehes selleks kindlaks energia ülekande elementaar-mehhanismid, mis vastutavad liitiumtetraboraadi rekombinatsioonluminestsentsi eest antud temperatuuride vahemikus.

Töö käigus saadi järgmised tulemused:

- Selgitati välja LTB:Ag, LTB:Cu,Ag, kristallide lisandikiirguse päritolu. Näidati, et esimesel juhul on kiirgusriba maksimumiga 4.6 eV juures põhjustatud Ag^+ iooni $5s \rightarrow 4d$ üleminekutega. Teoreetilised arvutused kasutades näitasid, et esmakordselt on selles töös leitud $4d \rightarrow 5s$ ja $4d \rightarrow 5d$ üleminekutele vastavad ergastusribad vastavalt 6.05 eV juures ja 7.0–7.7 eV piirkonnas. Näidati, et LTB:Cu,Ag kristalli korral kattub Ag^+ kiirgusriba 4.62 eV juures Cu^+ neelduvusspektri madalaima energia komponendiga 4.7 eV juures. Mis omakorda viitab, et Ag^+ ioonid sobivad Cu^+ kiirguse sensibiliseerimiseks. Energia ülekandele Ag^+ ioonidelt Cu^+ ioonidele LTB:Cu,Ag kristallis viitab selgelt Ag^+ ioonide poolt põhjustatud neeldumisõlg Cu^+ kiirgusele vastavas ergastusspektris 6.1 eV juures.
- LTB:Mn kristallide korral täheldati kahte Mn^{2+} seotud kiirgusriba. Esimene 2.03 eV juures on täheldatav värskest kasvatatud kristallides fotoergastusel ja kiiritatud kristallide termostimuleeritud luminestsentsis. Teine kiirgusriba 2.25–2.36 eV oli jälgitav kristallide korral, mida oli tsükliliselt kuumutatud ja kiiritatud. Kasvatatud kristallide ergastusspektris UV-vis piirkonnas esinevaid ergastusribasid seostati Mn^{2+} ioonide erinevate $3d^5$ elektronergastuste üleminekutega lahtuvalt Tanabe-Sugano diagrammist: Pakuti, et ergastusspektris täheldatud dublett 7.0 ja 7.5 eV juures vastab spinn-lubatud üleminekutele ning mis on kõige tõenäolisemalt seotud Mn^{2+} ioonide $3d^5 \rightarrow 3d^4 4s$ üleminekutega, mis asustavad 6D termi ning mis on kristallväljas lõhenenud kaheks alamribaks. On oluline märkida, et sellised ergastusribad mõõdeti LTB:Mn kristallide jaoks esmakordselt.
- EPR eksperimendid Q-sagedusribal LTB:Mn jaoks viidi läbi esmakordselt. Näidati, et enamasti siseneb mangaan kristalli kahevalentse ioonina ning asendab kristallvõres Li^+ iooni. Tulenevalt EPR tulemustest loodi mudel

mis seostab termostimuleeritud luminesentsi dosimeetrilises piigis kristallis toimuvate lisandi ümberlaadumise protsessidega.

- Näidati, et madalatel temperatuuridel röntgenkiite ja elektronidega otseergastuse korral domineerib puhta ja lisanditega kristalli röntgenluminesentsi ja katoodluminesentsi spektrites kiirgus, mis on tingitud laengukandjate rekombinatsioonist, kas häirimata võresõlmedel, või võresõlmedel, mis on häiritud lisandi iooni või mõne muu defekti poolt.
- Näidati, et LTB:Mn keraamikate kaaslisandamisel Cu^+ ionidega asub dosimeetriline piik samasuguses temperatuuride vahemikus nagu LTB:Mn korral. Samadel kiiritamistingimustel oli LTB:Mn,Cu integraalne intensiivsus kõrgem kui LTB:Mn korral, mis näitab, et kaaslisandamine Cu^+ ionidega suurendab materjali tundlikust ioniseeriva kiirguse suhtes.

ACKNOWLEDGEMENTS

I would like to thank my supervisor Dr. Vitali Nagirnyi for his continuous support, patience and advice during the years necessary to complete the present thesis. I am thankful for all the valuable, productive and memorable discussions.

I would like to express my gratitude to the Head of Laboratory of Physics of Ionic Crystals Prof. Aleksandr Lushchik for the possibility to carry out my research in this laboratory and for his continuous support.

I am grateful to Dr. Sebastian Vielhauer, Dr. Sergey Olmekov, and Dr. Dmitry Spassky for useful discussions and their technical help in carrying out the measurements in MAX-LAB and at the Institute of Physics, University of Tartu on different setups. D. Sc. László Kovács and Dr. Gábor Corradý from the Institute for Solid State Physics and Optics, Wigner Research Centre for Physics, Hungarian Academy of Science are thanked for providing the single crystal samples and Dr. Mihkel Kerikmäe and Dr. Mihkali Danilkin for preparing the ceramic samples. Special gratitude goes to Dr. V.V. Laguta, and Dr. Maksym Buryi from the Institute of Physics of the Czech Academy of Sciences, Prague, Czech Republic for useful discussions and for the help in interpreting the results obtained from EPR experiments and Prof. M. Brik from the Institute of Physics, University of Tartu, Estonia for the *ab-initio* calculations.

I wish to thank all the personnel from the Laboratory of Physics of Ionic Crystals for friendly atmosphere, support and advices that helped me tremendously throughout these years.

I am very thankful to my family and friends for their comprehensive support during my studies.

I appreciate the financial support received from the Estonian Research Council (grant IUT-2-26). This work was partially supported by the Graduate School “Functional materials and technologies” (project 1.2.0401.09-0079) and also by ASTRA project PER ASPERA, Graduate School of Functional Materials and Technologies, receiving funding from the European Regional Development Fund under project in University of Tartu, Estonia. I also acknowledge a partial financial support from the Estonian Centre of Excellence TK141 by the EU through the European Regional Development Fund (TK141 “Advanced materials and high-technology devices for sustainable energetics, sensorics and nanoelectronics”, project No. 2014-2020.4.01.15-0011). This work was also supported by the Cooperation Program between Estonian and Hungarian Academies of Science. I appreciate the support from national scholarship program Kristjan Jaak, which is funded and managed by Archimedes Foundation in collaboration with the Ministry of Education and Research.

REFERENCES

- [1] F. Daniels, C.A. Boyd, and D.F. Saunders, *Science* 117 (1953) 343.
- [2] A.C. Fernandes, M. Osvay, J.P. Santos, V. Holovey, M. Ignatovych, *Radiat. Meas.* 43 (2008) 476.
- [3] O. Annalakshmi, M.T. Jose, G. Amarendra. *Radiation Measurements* 46 (2011) 669.
- [4] N. Can, T. Karali, P.D. Townsend, F. Yıldız, *J. Phys. D Appl. Phys.* 39 (2006) 2038.
- [5] R.H. French, J.W. Ling, F.S. Ohuchi, C.T. Chen, *Phys. Rev. B*, 44 (16) (1991) 8496.
- [6] R. Komatsu, T. Sugawara, K. Sassa, N. Sarukura, Z. Liu, S. Izumida, Y. Segawa, S. Uda, T. Fukuda and K. Yamanouchi, *Appl. Phys. Lett.* 70 (1997) 3492.
- [7] P. Becker, "Borate Materials in Nonlinear Optics", *Adv. Mater.*, 10 (13) (1998) 979.
- [8] I.N. Ogorodnikov, V.A. Pustovarov, A.V. Kurzhalov, L.I. Isaenko, M. Kirm and G. Zimmerer, *Phys. Solid State* 42 (3) (2000) 464.
- [9] S. Furusawa, O. Chikagawa, S. Tange, T. Ishidate, H. Orihara, Y. Ishibashi and K. Miwa, *J. Phys. Soc. Japan*, 60 (1991) 2691.
- [10] G.C. Bhar, A.K. Chaudhary, P. Kumbhakar, and A.M. Rudra, *J. Phys. D: Appl. Phys.* 34 (2001) 360.
- [11] V. Petrov, F. Rotermund, F. Noack, R. Komatsu, T. Sugawara, and S. Uda, *J. Appl. Phys.* 84 (1998) 5887.
- [12] V. Petrov, F. Rotermund, F. Noack, J. Ringling, O. Kittelmann, and R. Komatsu, *IEEE J. Sel. Top. Quantum Electron.* 5 (1999) 1532.
- [13] R.W. Whatmore, N.M. Shorrocks, C. O'Hara, F.W. Ainger and I.M. Young, *Electron. Lett.* 17 (1981) 11.
- [14] Y. Ebata, H. Suzuki, S. Matsumura and K. Fukuda, *Jpn. J. Appl. Phys.*, 22-2 (Suppl.) (1983) 160.
- [15] K. Otsuka, M. Funami, M. Ito, H. Katsuda, M. Tacano, M. Adachi and A. Kawabata, *J. Appl. Phys.* 34 (1995) 2646.
- [16] A.S. Bhalla, L.E. Cross and R.W. Whatmore, *Jpn. J. Appl. Phys.* 24 (1985) 727.
- [17] M. Ono, M. Sakai, Y. Fujiwara and N. Wakatsuki, *Proc. 1997 IEEE Ultrasonics Symp.* vol 2, (Toronto) (1997) p 1047.
- [18] C-S. Kim, J-H. Park, B.K. Moon, H-J. Seo, B-Ch. Choi, Y-H. Hwang, H.K. Kim and J.N. Kim, *J. Appl. Phys.* 94 (2003) 7246.
- [19] C-S. Kim, D.J. Kim, Y-H. Hwang, H.K. Kim and J.N. Kim, *J. Appl. Phys.* 92 (2002) 4644.
- [20] I.M. Rizak, V.M. Rizak, N.D. Baisa, V.S. Bilanich, M.V. Boguslavskiî, S.Yu. Stefanovich and V.M. Goloveî, *Crystallogr. Rep.* 48 (2003) 676.
- [21] D.P. Button, L.S. Mason, H.L. Tuller, D.R. Uhlmann, *Solid State Ionics* 9-10 (1983) 585.
- [22] J.H. Schulman, R.D. Kirk, E.J. West, *Proc. 1st Int. Conf. Lumin. Dosim.* (1967) 113.
- [23] M. Takenaga, O. Yamamoto, T. Yamahita, *Nucl. Instrum. Methods* 175 (1980) 77.
- [24] M. Prokic, *Radiat. Prot. Dosim.* 100 (2002) 265-268.
- [25] M. Martini, F. Meinardi, L. Kovacs, and K. Polgar, *Radiat. Prot. Dosim.* 65 (1996) 343.

- [26] K. Sangeta, D.G. Chennakesavulu, S.C. Desai, Mary Alex, M.D. Ghodgaonkar, Nucl. Instrum. Methods Phys. Res. A, 571 (2007) 699.
- [27] T. Nakamura, M. Katagiri, Y.E. Chen, M. Ukibe, and M. Ohkubo, Nucl. Instrum. Methods Phys. Res., Sect A 559 (2006) 766.
- [28] Ya.V. Burak, V.T. Adamiv, I.M. Teslyuk, V.M. Shevel, Radiat. Meas. 38 (2004) 681.
- [29] Y. Kutomi and N. Takeuchi, J. Mater. Sci. Lett. 5 (1986) 51-53.
- [30] C. Furetta, M. Prokic, R. Salamon, V. Prokic, G. Kitis, Nucl. Instrum. Methods Phys. Res., Sect. A 456 (2001) 411.
- [31] C.A. Jaychandran, Phys. Med. Biol. 16 (1971) 617.
- [32] J.G. Gualtieri, J.A. Kosinski, W.D. Wilber, Y. Lu, S.T. Lin, M. Murray, and W. Ruderman, Proceedings of 1992 IEEE Frequency Control Symposium, Hershey, USA, 1992, p. 724.
- [33] J. Krogh-Moe, Acta Crystallogr. 15 (1962) 190.
- [34] T.Y. Kwon, J.J. Ju, H.K. Kim, D.J. Kim, J.W. Cha, J.N. Kim, S.I. Yun, M. Cha, Mater. Lett. 30 (1997) 293.
- [35] T.Y. Kwon, J.J. Ju, J.W. Cha, J.N. Kim, S.I. Yun, Mater. Lett. 20 (1994) 211.
- [36] D. London, M.E. Zolensky, E. Roedder, The Canadian Mineralogist 25 (1987) 173.
- [37] B.S. R. Sastry and F.A. Hummel, J. Am. Ceram. Soc. 41 (1958) 7.
- [38] J. Krogh-Moe, Acta Crystallogr., Sect. B Struct. Sci. 24 (1968) 179.
- [39] S.F. Radaev, L.A. Muradyan, L.F. Malakhova, Ya.V. Burak, and V.I. Simonov, Kristallografiya 34 (1989) 1400.
- [40] M. Natarajan, R. Faggiani and I. D. Brown, Cryst. Struct. Commun. 8 (1979) 367.
- [41] N. Sennova, R. Bubnova, J. Shepelev, S. Filatov, O. Yakovleva, J. Alloys Compd. 428 (2007) 290.
- [42] A. Senyshyn, B. Schwarz, T. Lorenz, V.T. Adamiv, Ya.V. Burak, J. Banys, R. Grigalaitis, L. Vasylechko, H. Ehrenberg and H. Fuess, J. Appl. Phys. 108 (2010) 093524.
- [43] A. Senyshyn, H. Boysen, R. Niewa, J. Banys, M. Kinka, Ya. Burak, V. Adamiv, F. Izumi, I. Chumak and H. Fuess, J. Phys. D: Appl. Phys. 45 (2012) 175305.
- [44] O.T. Antonyak, Ya.V. Burak, I.T. Lyseiko, M.S. Pidzyrailo, Z.A. Khapko, Opt. Spectrosc. 61 (1986) 345.
- [45] G. Corradi, V. Nagirnyi, A. Kotlov, A. Watterich, M. Kirm, K. Polgár, A. Hofstaetter, M. Meyer, J. Phys. Condens. Matter. 20 (2008) 025216.
- [46] B. Tiwari, N.S. Rawat, D.G. Desai, S.G. Singh, M. Tyagi, P. Ratna, S.C. Gadkari, M. S. Kulkarni, J. Lumin. 130 (2010) 2076.
- [47] M. Ignatovych, M. Fasoli, A. Kelemen, Radiat. Phys. Chem. 81 (2012) 1528.
- [48] B.T. Huy, V.X. Quang, H.T.B. Chau, J. Lumin. 128 (2008) 1601.
- [49] V. Burak, V.T. Adamiv, O.T. Antonyak, S.Z. Malynych, M.S. Pidzyrailo, I. M. Teslyuk, Ukr. J. Phys. 50 (2005) 1153.
- [50] A. (Türkler) Ege, E. Ekdal, T. Karali, N. Can, Radiat. Meas. 42 (2007) 1280.
- [51] M. Ignatovych, V. Holovey, A. Watterich, T. Vidoczy, P. Baranyai, A. Kelemen, O. Chuiko, Funct. Mater. 12 (2005) 313.
- [52] M. Ignatovych, V. Holovey, T. Vidóczy, P. Baranyai, A. Kelemen, Radiat. Phys. Chem. 76 (2007) 1527.
- [53] G.D. Patra, M. Tyagi, D.G. Desai, B. Tiwari, S. Sen, S.C. Gadkari, J. Lumin. 132 (2012) 1101.

- [54] T. Brant, B.E. Kananen, M.K. Murari, J.W. McClory, J.C. Petrosky, V.T. Adamiv, Ya.V. Burak, P.A. Dowben, L.E. Halliburton, *J. Appl. Phys.* 110 (2011) 093719.
- [55] Z. Xiong, Q. Tang, X. Xiong, D. Luo, P. Ding, *Radiat. Meas.* 46 (2011) 323.
- [56] D. Podgórska, S.M. Kaczmarek, W. Drozdowski, W. Wabia, M. Kwasny, S. Warchoń, V.M. Rizak, *Mol. Phys. Rep.* 39 (2004) 199.
- [57] D. Podgórska, S.M. Kaczmarek, W. Drozdowski, M. Wabi, M. Kwasny, S. Warchoń, V.M. Rizak, *Acta Phys. Polonica* 107 (2005) 507.
- [58] S. Kar, Sunil Verma, K.S. Bartwal, *Physica B* 405 (2010) 4299.
- [59] V.M. Holovey, V.I. Lyamayev, M.M. Birov, P.P. Puga, A.M. Solomon., *Functional Materials* 12/2 (2005) 318.
- [60] V.M. Holovey, K.P. Popovich, D.B. Goyer, V.M. Krasyllynets, A.V. Gomonnai, *Radiat. Eff. Defects Sol.* 166/7 (2011) 522.
- [61] J. Manam, S. K. Sharma, *Radiat. Eff. Defects Sol.* 163 (2008) 813.
- [62] O. Annalakshmi, M.T. Jose, U. Madhusoodanan, B. Venkatraman, G. Amarendra. *J. Lumin.* 141 (2013) 60.
- [63] M. Danilkin, I. Jaek, M. Kerikmäe, A. Lust, H. Mändar, L. Pung, A. Ratas, V. Seeman, S. Klimonsky, V. Kuznetsov, *Radiat. Meas.* 45 (2010) 562.
- [64] A. Ratas, M. Danilkin, M. Kerikmäe, A. Lust, H. Mändar, V. Seeman, G. Slavin, *Proc. Est. Acad. Sci., Materials Sci.* 61/4 (2012) 279.
- [65] B.V. Padlyak, W. Wojtowicz, V.T. Adamiv, Ya.V. Burak, I.M. Teslyuk, *Acta Phys. Pol. A* 117 (2010) 122.
- [66] T.D. Kelly, L. Kong, D.A. Buchanan, A.T. Brant, J. Petrosky, J.W. McClory, V.T. Adamiv, Ya.V. Burak, P. Dowben, *Phys. Stat. Sol. (b)* 250/7 (2013) 1376.
- [67] A. Kelemen, M. Ignatovych, V. Holovey, T. Vidoczy, P. Baranya, *Radiat. Phys. Chem.* 76 (2007) 1531.
- [68] S. Kar, S. Bairagi, C. Debnath, S. Verma, K.S. Bartwal, *Appl. Phys. Lett.* 101 (2012) 071904.
- [69] G. Zimmerer, *Radiat. Meas.* 42 (2007) 859.
- [70] S. Urpelainen, M. Huttula, T. Balasubramanian, R. Sankari, P. Kovala, E. Kukk, E. Nömmiste, S. Aksela, R. Nyholm, H. Aksela, *AIP Conf. Proc.* 1234 (2010) 441.
- [71] A. Tuomela, V. Pankratov, A. Sarakovskis, G. Doke, L. Grindberga, S. Vielhauer, M. Huttula, *J. Lumin.* 179 (2016) 16.
- [72] E. Feldbach, A. Kotlov, I. Kudryavtseva, P. Liblik, A. Lushchik, A. Maaros, I. Martinson, V. Nagirnyi, E. Vasil'chenko, *Nucl. Instrum. Methods Phys. Res. B* 250 (2006) 159.
- [73] E. Feldbach, E. Töldsepp, M. Kirm, A. Lushchik, K. Mizohata, J. Räisänen, *Opt. Mater.* 55(2016) 164.
- [74] M. Ignatovych, V. Holovey, A. Watterich, T. Vidoczy, P. Baranyai, A. Kelemen, V. Ogenko, O. Chuiko, *Radiat. Phys. Chem.* 67 (2003) 587.
- [75] G.D. Patra, S.G. Singh, B. Tiwari, S. Sen, D.G. Desai, S.C. Gadkari, *J. Lumin.* 137 (2013) 28.
- [76] V. Nagirnyi, A. Kotlov, G. Corradi, A. Watterich and M. Kirm, *Phys. Stat. Sol. (C)* 4 (2007) 885.
- [77] G. Corradi, V. Nagirnyi, A. Kotlov, A. Watterich, K. Polgár, *J. Phys. : Conf. Ser.* 249 (2010) 012008.
- [78] M.D. Segall, P.J.D. Lindan, M.J. Probert, C.J. Pickard, P.J. Hasnip, S.J. Clark, M. C. Payne, *J. Phys. Condens. Matter.* 14 (2002) 2717.
- [79] J.P. Perdew, K. Burke, M. Ernzerhof, *Phys. Rev. Lett.* 77 (1996) 3865.

- [80] M. Nazarov, M.G. Brik, D. Spassky, B. Tsukerblat, A. Nor Nazida, M.N. Ahmad-Fauzi, J. Alloy. Compd. 573 (2013) 6.
- [81] J. Sugar and C. Corliss, Atomic Energy Levels of the Iron-Period Elements: Potassium through Nickel, J. Phys. Chem. Ref. Data 14, Suppl. 2, 1–664 (1985).
- [82] S. Kück, I. Sokólska, J. Phys.: Condens. Matter 18 (2006) 5447-5457.
- [83] A. El-Korashy, M.G. Brik, Solid State Commun. 135 (2005) 298.
- [84] Wu Shao-Yi, Zheng Wen-Chen, Physica B 296 (2001) 351.
- [85] Zheng Wen-Chen, Wu Shao-Yi, Physica B 271 (1999) 252.
- [86] U. Hålenius, F. Bosi, H. Skogby, American Mineralogist 92 (2007) 1225.
- [87] D. Möncke, E.I. Kamitsos, A. Herrmann, D. Ehrt, M. Friedrich, J. Non-Cryst. Solids 357 (2011) 2542.
- [88] J. Barzowska, Zhiguo Xia, D. Jankowski, D. Włodarczyk, K. Szczodrowski, Chong-Geng Ma, M.G. Brik, Ya. Zhydashchevskii and A. Suchocki, RSC Adv. 7 (2017) 275.
- [89] S.A. Altshuler, B.M. Kozyrev, Electron Paramagnetic Resonance in Compounds of Transition Elements, 2nd ed.; John Wiley & Sons, Inc.: New York, NY, USA (1974).
- [90] C.P. Poole Jr., H.A. Farach Eds., Handbook of Electron Spin Resonance, Vol. 2; Springer-Verlag, AIP Press, New York, NY, USA, (1999).
- [91] J.E. Wertz, J.R. Bolton, Electron spin resonance. Elementary theory and practical applications, McGraw-Hill, Inc, (1972).
- [92] S. Stoll, A. Schweiger, EasySpin, a comprehensive software package for spectral simulation and analysis in EPR, J. Magn. Reson., 42 (2006) 178.
- [93] R.D. Shannon, Acta Crystallogr. A, 32 (1976) 751.
- [94] V.M. Holovey, V.I. Sidey, V.I. Lyamayev, P.P. Puga, J. Lumin. 126 (2007) 408.
- [95] G. Kitis, J.M. Gomez-Ros, J.W.N. Tuyn, J. Phys. D Appl. Phys. 31 (1998) 2636.
- [96] V. Kiisk, Radiat. Prot. Dosim., 156(3) (2013) 261.
- [97] M.W. Swinney, J.W. McClory, J.C. Petrosky, Shan Yang, A.T. Brant, V.T. Adamiv, Ya.V. Burak, P.A. Dowben, L.E. Halliburton, J. Appl. Phys. 107 (2010) 113715.
- [98] D.I. Griscom, P.C. Taylor, D.A. Ware, and P.J. Bray, The Journal of Chemical Physics 48 (11) (1968) 5158.
- [99] K.Ya. Borman, Ya.V. Burak, I.T. Perro, M.A. Kundzinsh, I.T. Lyseiko, Current Problems in Physics and Chemistry of Ferroelectrics, Riga, 140, (1987).
- [100] V.V. Zaretskii, Y.V. Burak, Fiz. Tverd. Tela 31 (6) (1989) 80.
- [101] V.V. Zaretskii, Y.V. Burak, JETP Lett. 49 (4) (1989) 229.
- [102] N. D. Zhigadlo, Phys. Status Solidi A 152 (1995) 329.
- [103] N.P. Tekhanovich, A.U. Sheleg, Ya.V. Burak, Fiz. Tverd. Tela 32 (1990) 2513.
- [104] I. Ketsman, D. Wooten, Jie Xiao, Ya.B. Losovyj, Ya.V. Burak, V.T. Adamiv, A. Sokolov, J. Petrosky, J. McClory, P.A. Dowben, Phys. Lett. A 374 (2010) 891.
- [105] A.A. Seher, D.J. Somerford, J. Phys. Condens. Matter 1 (1989) 2279.
- [106] C.E. Weir, R.A. Schroeder, J. Res. NBS A 68 (1963) 465.
- [107] C.N.R. Rao, H.S. Randhawa, N.V.R. Reddy, D. Chakravorty, Spectrochim. Acta A 31 (1975) 1283.
- [108] N.D. Zhigadlo, M. Zhang, E.K.H. Salje, J. Phys. Condens. Matter 13 (2001) 6551.
- [109] V.V. Maslyuk, T. Bredow, H. Pfnür, Eur. Phys. J. B 42 (2004) 461.
- [110] A.T. Brant, D.A. Buchanan, J.W. McClory, P.A. Dowben, V.T. Adamiv, Ya.V. Burak, L.E. Haliburton, J. Lumin. 139 (2013) 125.

- [111] J. T. Randall, M. H. F. Wilkins, *Proc. R. Soc. Lond. A* 184 (1945) 365.
- [112] D.A. Buchanan, M.S. Holston, A.T. Brant, J.W. McClory, V.T. Adamiv, Ya.V. Burak, L.E. Halliburton, *J. Phys. Chem. Solids* 75 (2014) 1347.
- [113] A.T. Brant, D.A. Buchanan, J.W. McClory, V.T. Adamiv, Ya.V. Burak, L. E. Haliburton, N.C. Giles, *J. Lumin.* 153 (2014) 79.
- [114] J.K. Srivastava, S.J. Supe, *Nucl. Instrum. Methods.* 160 (1979) 529.
- [115] L. Singh, V. Chopra, S.P. Lochab, *J. Lumin.* 131 (2011) 1177.
- [116] Ch. Dugan, R.L. Hengehold, S.R. McHale, J.A. Colon Santana, J.W. McClory, V.T. Adamiv, Ya.V. Burak, Ya.B. Losovyj, P.A. Dowben, *Appl. Phys. Lett.* 102 (2013) 161602.
- [117] F. Williams, *Phys. Stat. Sol.* 25 (1968) 493.
- [118] C. Guarneros-Aguilar, E. Cruz-Zaragoza, J. Marcazzó, R. Palomino-Merino, J.E. Espinosa, *AIP Conf. Proc.* 1544 (2013) 70.

PUBLICATIONS

CURRICULUM VITAE

Name: Ivo Romet
Date of birth: 21.05.1985
Citizenship: Estonian
Phone: +372 5648 4295
E-mail: ivo.romet@ut.ee

Current position: Laboratory of Physics of Ionic crystals, Institute of Physics, University of Tartu, Junior Research Fellow of Solid State Physics

Education:

2012-present University of Tartu, PhD studies
2009–2011 University of Tartu, Materials Science, MSc
2005–2009 University of Tartu, Materials Science BSc
2001–2004 Oskar Lutsu Palamuse Gymnasium
1992–2001 J.V. Veski Maarja Elementary School

Language skills:

Estonian mother tongue
English good
German good
Russian good

Institution and position held:

2016 – University of Tartu, Faculty of Science and Technology, Institute of Physics, Laboratory of Physics of Ionic Crystals, Junior Research Fellow of Solid State Physics
2012–2015 University of Tartu, Faculty of Science and Technology, Institute of Physics, engineer
2007–2007 University of Tartu, Faculty of Science and Technology, Institute of Physics, laboratory technician

Research interests:

Solid state physics, scintillation materials, steady state and time-resolved optical spectroscopy, thermoluminescence and radiation physics of ionic crystals.

Publications:

- I. Romet**, M. Buryi, G. Corradi, E. Feldbach, V. Laguta, É. Tichy-Rács, V. Nagirnyi, “Recombination luminescence and EPR of Mn doped of $\text{Li}_2\text{B}_4\text{O}_7$ single crystals”, *Optical Materials*, accepted manuscript.
V. Kortov, A. Lushchik, V. Nagirnyi, D. Ananchenko, **I. Romet**, “Spectrally resolved thermally stimulated luminescence of irradiated anion-defective alumina single crystals”, *Journal of Luminescence*, **186** (2017) 189–193.

- I.E. Seferis, K. Fiaczky, D. Spassky, E. Feldbach, **I. Romet**, M. Kirm, E. Zych, "Synthesis and luminescence properties of BaHfO₃:Pr ceramics", *Journal of Luminescence*. In Press: <http://dx.doi.org/10.1016/j.jlumin.2016.09.035>
- I. Romet**, E. Aleksanyan, M.G. Brik, G. Corradi, A. Kotlov, V. Nagirnyi, K. Polgár, "Recombination luminescence of Cu and/or Ag doped lithium tetraborate single crystals", *Journal of Luminescence* **177** (2016) 9–16.
- A. Kuznetsov, A. Frorip, J. Kozlova, V. Nagirnyi, M. Ots-Rosenberg, **I. Romet**, A. Sünter, "Visible fluorescence of biological fluids as a renal failure marker: New integrative approach", *Journal of Innovative Optical Health Sciences* **8** (4) (2015) 1550030.
- M. Kerikmäe, M. Danilkin, A. Lust, V. Nagirnyi, L. Pung, A. Ratas, **I. Romet**, V. Seeman, "Hole traps and thermoluminescence in Li₂B₄O₇:Be", *Radiation Measurements* **56** (2013) 147–149.
- V. Nagirnyi, E. Aleksanyan, G. Corradi, M. Danilkin, E. Feldbach, M. Kerikmäe, A. Kotlov, A. Lust, K. Polgár, A. Ratas, **I. Romet**, V. Seeman, "Recombination luminescence in Li₂B₄O₇ doped with manganese and copper", *Radiation Measurements* **56** (2013) 192–195.

Conference presentations:

- I. Romet**, G. Corradi, M. Danilkin, M. Kerikmäe, A. Kotlov, V. Nagirnyi, V. Seeman, "Recombination luminescence in Li₂B₄O₇ doped with manganese and copper". Poster presentation at the 8th International conference Functional Materials and Nanotechnologies (FMNT), 2013, Tartu, Estonia.
- I. Romet**, M.G. Brik, G. Corradi, M. Danilkin, M. Kerikmäe, A. Kotlov, V. Nagirnyi "Thermally and optically stimulated luminescence in Li₂B₄O₇ doped with silver". Poster presentation at the Functional Materials and Technologies Graduate School Conference (FMTDK), 2014, Tartu, Estonia.
- I. Romet**, M.G. Brik, G. Corradi, M. Danilkin, M. Kerikmäe, A. Kotlov, V. Nagirnyi, "Thermally and optically stimulated luminescence in Li₂B₄O₇ doped with silver". Poster presentation at the 12th Europhysical Conference on Defects in Insulating Materials (EURODIM), 2014, Canterbury, United Kingdom.
- I. Romet**, G. Corradi, A. Kotlov, K. Lengyel, V. Nagirnyi, "Low temperature luminescence in Li₂B₄O₇ doped with Cu, Ag and Mn ions". Poster presentation at the 9th International Conference on Luminescent Detectors and Transformers of Ionizing Radiation (LUMDETR), 2015, Tartu, Estonia.
- I. Romet**, E. Tichy-Racs, L. Kovacs, K. Lengyel, G. Corradi, V. Nagirnyi, I. Hajdara, "Optical spectroscopy of Li₆Y(BO₃)₃ single crystals doped with dysprosium". Poster presentation at the 9th International Conference on Luminescent Detectors and Transformers of Ionizing Radiation (LUMDETR), 2015, Tartu, Estonia.
- I. Romet**, E. Aleksanyan, M.G. Brik, G. Corradi, A. Kotlov, V. Nagirnyi, K. Polgár, "Recombination luminescence of copper and silver doped Li₂B₄O₇ single crystal". Poster presentation at the 19th International Conference on Defects in Insulating Materials (ICDIM), 2016, Lyon, France.

Awards and scholarships:

- 2014 Functional Materials and Technologies Graduate School travel scholarship to attend 12th Europhysical Conference on Defects in Insulating Materials (EURODIM 2014).
- 2016 Kristjan Jaak's program scholarship to attend the 19th International Conference on Defects in Insulating Materials (ICDIM 2016).

ELULOOKIRJELDUS

Nimi: Ivo Romet
Sünniaeg: 21.05.1985
Kodakondsus: Eesti
Telefon: +372 5648 4295
E-post: ivo.romet@ut.ee

Praegune töökoht: Ioonkristallide füüsika labor, Füüsika Instituut, Tartu Ülikool, nooremteadur

Haridus:

2012-k. a. Tartu Ülikool, doktoriõpe
2009–2011 Tartu Ülikool, Materjaliteadus, MSc
2005–2009 Tartu Ülikool, Materjaliteadus BSc
2001–2004 Oskar Lutsu Palamuse Gümnaasium
1992–2001 J. V. Veski nim. Maarja Põhikool

Keelteoskus:

Eesti keel emakeel
Inglise keel hea
Saksa keel hea
Vene keel hea

Teenistuskäik:

2016– Tartu Ülikool, Füüsika Instituut, Ioonkristallide füüsika labor, tahkisefüüsika nooremteadur
2012–2015 Tartu Ülikool, Loodus- ja teadustehnoloogiateaduskond, Füüsika Instituut, insener
2007–2007 Tartu Ülikool, Loodus- ja teadustehnoloogiateaduskond, Füüsika Instituut, laborant

Peamised uurimisvaldkonnad:

Tahke keha füüsika, stsintillatsioonmaterjalid, statsionaarne ja aeglahutusega optiline spektroskoopia, termostimuleeritud luminesents ja ioonkristallide kiiritusfüüsika.

Publikatsioonid:

I. Romet, M. Buryi, G. Corradi, E. Feldbach, V. Laguta, É. Tichy-Rács, V. Nagirnyi, “Recombination luminescence and EPR of Mn doped Li₂B₄O₇ single crystals”, *Optical Materials*, accepted manuscript.
V. Kortov, A. Lushchik, V. Nagirnyi, D. Ananchenko, **I. Romet**, “Spectrally resolved thermally stimulated luminescence of irradiated anion-defective alumina single crystals”, *Journal of Luminescence*, **186** (2017) 189–193.

- I. E. Seferis, K. Fiaczky, D. Spassky, E. Feldbach, **I. Romet**, M. Kirm, E. Zych, "Synthesis and luminescence properties of BaHfO₃:Pr ceramics", *Journal of Luminescence*. In Press: <http://dx.doi.org/10.1016/j.jlumin.2016.09.035>
- I. Romet**, E. Aleksanyan, M.G. Brik, G. Corradi, A. Kotlov, V. Nagirnyi, K. Polgár, "Recombination luminescence of Cu and/or Ag doped lithium tetraborate single crystals", *Journal of Luminescence*, **177** (2016) 9–16.
- A. Kuznetsov, A. Frorip, J. Kozlova, V. Nagirnyi, M. Ots-Rosenberg, **I. Romet**, A. Sünter, "Visible fluorescence of biological fluids as a renal failure marker: New integrative approach", *Journal of Innovative Optical Health Sciences*, **8** (4) (2015) 1550030.
- M. Kerikmäe, M. Danilkin, A. Lust, V. Nagirnyi, L. Pung, A. Ratas, **I. Romet**, V. Seeman, "Hole traps and thermoluminescence in Li₂B₄O₇:Be", *Radiation Measurements*, **56** (2013) 147–149.
- V. Nagirnyi, E. Aleksanyan, G. Corradi, M. Danilkin, E. Feldbach, M. Kerikmäe, A. Kotlov, A. Lust, K. Polgár, A. Ratas, **I. Romet**, V. Seeman, "Recombination luminescence in Li₂B₄O₇ doped with manganese and copper", *Radiation Measurements*, **56** (2013) 192–195.

Konverentsiettekanded:

- I. Romet**, G. Corradi, M. Danilkin, M. Kerikmäe, A. Kotlov, V. Nagirnyi, V. Seeman, "Recombination luminescence in Li₂B₄O₇ doped with manganese and copper". Stendiettekanne konverentsil "8th International conference Functional Materials and Nanotechnologies", 2013, Tartu, Eesti.
- I. Romet**, M.G. Brik, G. Corradi, M. Danilkin, M. Kerikmäe, A. Kotlov, V. Nagirnyi "Thermally and optically stimulated luminescence in Li₂B₄O₇ doped with silver". Stendiettekanne Funktsionaalsete materjalide ja tehnoloogiate doktorikooli teaduskonverentsil, 2014, Tartu, Eesti.
- I. Romet**, M.G. Brik, G. Corradi, M. Danilkin, M. Kerikmäe, A. Kotlov, V. Nagirnyi, "Thermally and optically stimulated luminescence in Li₂B₄O₇ doped with silver". Stendiettekanne konverentsil "12th Europhysical Conference on Defects in Insulating Materials", 2014, Canterbury, Suurbritannia.
- I. Romet**, G. Corradi, A. Kotlov, K. Lenglyel, V. Nagirnyi, "Low temperature luminescence in Li₂B₄O₇ doped with Cu, Ag and Mn ions". Stendiettekanne konverentsil "9th International Conference on Luminescent Detectors and Transformers of Ionizing Radiation", 2015, Tartu, Eesti.
- I. Romet**, E. Tichy-Racs, L. Kovacs, K. Lengyel, G. Corradi, V. Nagirnyi, I. Hajdara, "Optical spectroscopy of Li₆Y(BO₃)₃ single crystals doped with dysprosium.". Stendiettekanne konverentsil "9th International Conference on Luminescent Detectors and Transformers of Ionizing Radiation", 2015, Tartu, Eesti.
- I. Romet**, E. Aleksanyan, M.G. Brik, G. Corradi, A. Kotlov, V. Nagirnyi, K. Polgár, "Recombination luminescence of copper and silver doped Li₂B₄O₇ single crystal". Stendiettekanne konverentsil "19th International Conference on Defects in Insulating Materials", 2016, Lion, Prantsusmaa.

Saadud uurimistoetused ja stipendiumid:

- 2014 Funktsionaalsete materjalide ja tehnoloogiate doktorikooli reisistipendium osalemiseks konverentsil “12th Europhysical Conference on Defects in Insulating Materials (EURODIM 2014)”.
- 2016 Kristjan Jaagu välissõidu stipendium osalemiseks konverentsil “19th International Conference on Defects in Insulating Materials (ICDIM 2016)”.

DISSERTATIONES SCIENTIAE MATERIALIS UNIVERSITATIS TARTUENSIS

1. **Martin Järvekülg.** Tubular microstructures by Hf-, Zr- and Ti-butoxide gel sheet rolling. Tartu, 2011, 112 p.
2. **Sergei Vlassov.** Investigation of nanoscale interactions and mechanical properties of nanostructures using quartz tuning fork based real-time measurements. Tartu, 2011, 171 p.
3. **Margus Kodu.** Pulsed Laser Deposition of Magnesium Oxide and Barium Ternary Oxides for Plasma Display Protective Layers. Tartu, 2011, 89 p.
4. **Rainer Pärna.** Surface studies of some oxide films. Tartu, 2011, 129 p.
5. **Jevgeni Šulga.** Self-assembly and interaction of nanostructures. Tartu, 2011, 114 p.
6. **Wojciech Kuznik.** Quantum-chemical computer simulations of the linear and non-linear optical properties of pyrazoloquinoline and dicyanopyrazine derivatives. Tartu, 2012, 89 p.
7. **Leonid Dorogin.** Structural and tribological properties of zero- and one-dimensional nanocrystals. Tartu, 2012, 193 p.
8. **Viljar Palmre.** Fabrication and characterization of microporous carbon-based electroactive polymer actuators. Tartu, 2012, 99 p.
9. **Madis Paalo.** Synthesis of CNT-metal oxide nanocomposites: sol-gel process, rheology, structural and functional properties. Tartu, 2014, 175 p.
10. **Raul Välbe.** Development of ionic liquid composites by sol-gel method for elaboration of industrial nano- and microstructures. Tartu, 2014, 97 p.
11. **Urmas Joost.** Impurity and preparation dependent properties of titania thin films. Tartu, 2014, 155 p.
12. **Madis Umalas.** Application of sol-gel technology for production of ceramic nanocomposites and functional coatings. Tartu, 2015, 136 p.
13. **Elena Samsonova.** Energy transfer probe as a tool to study morphological and structural origins of fluorescence quenching in rare-earth doped nanophosphors. Tartu, 2015, 114 p.
14. **Jay Mondal.** Novel Corrosion Protective Nanostructured Composite Coatings. Tartu, 2016, 104 p.
15. **Kathriin Utt.** Metal oxide mesostructures for optical applications. Tartu, 2016, 88 p.
16. **Kaido Siimon.** Electrospun gelatin cross-linked by glucose. Tartu, 2016, 84 p.
17. **Marko Part.** Combined three-dimensional sol-gel structures and atomic layer deposited thin films. Tartu, 2017, 162 p.
18. **Pejman Rasti.** Analysis of Remote Sensing Image Super Resolution using Fluid Lenses. Tartu, 2017, 188 p.